Space Weather

Key Points:
- Similar yet distinct enhancements in the TEC at Bharati and Davis during both the storms are associated with the formation of TOI/SEDs
- IT response led by the strong and sustained magnetopause erosion led to enhanced plasma content in the SEDs on 17 March 2015
- External driving mechanisms played an important role in modulating the high-mid latitude space weather

Correspondence to:
P. R. Shreedevi,
shreedevipr@gmail.com

Geomagnetic Storm-Induced Plasma Density Enhancements in the Southern Polar Ionospheric Region: A Comparative Study Using St. Patrick's Day Storms of 2013 and 2015

P. R. Shreedevi[1,2] [iD], **R. K. Choudhary[2]** [iD], **Smitha V. Thampi[2]** [iD], **Sneha Yadav[2]** [iD], **T. K. Pant[2]** [iD], **Yiqun Yu[1]** [iD], **Ryan McGranaghan[3]** [iD], **Evan G. Thomas[4]** [iD], **Anil Bhardwaj[5]** [iD], and **A. K. Sinha[6]** [iD]

[1]School of Space and Environment, Beihang University, Beijing, China, [2]Space Physics Laboratory, Vikram Sarabhai Space Centre, Thiruvananthapuram, India, [3]Atmosphere and Space Technology Research Associates (ASTRA), LLC, Louisville, CO, USA, [4]Thayer School of Engineering, Dartmouth College, Hanover, NH, USA, [5]Physical Research Laboratory, Ahmedabad, India, [6]Indian Institute of Geomagnetism, New Bombay, India

Abstract The occurrence of St. Patrick's Day (17 March) geomagnetic storms during two different years (2013 and 2015) with similar solar flux levels but varying storm intensity provided an opportunity to compare and contrast the responses of the ionosphere-thermosphere (IT) system to different levels of geomagnetic activity. The evolution of positive ionospheric storms at the southern polar stations Bharati (76.6°S MLAT) and Davis (76.2°S MLAT) and its causative connection to the solar wind driving mechanisms during these storms has been investigated in this paper. During the main phase of both the storms, significant enhancements in TEC and phase scintillation were observed in the magnetic noon/ midnight period at Bharati and Davis. The TEC in the midnight sector on 17 March 2015 was significantly higher compared to that on 17 March 2013, in line with the storm intensity. The TEC enhancements during both the storm events are associated with the formation of the storm-enhanced densities (SEDs)/tongue of ionization (TOI). The strong and sustained magnetopause erosion led to the prevalence of stronger storm time electric fields (prompt penetration electric field (PPEF)/subauroral polarization streams (SAPS)) for long duration on 17 March 2015. This combined with the action of neutral winds at midlatitudes favored the formation of higher plasma densities in the regions of SED formation on this day. The same was weaker during the 17 March 2013 storm due to the fast fluctuating nature of interplanetary magnetic field (IMF) B_z. This study shows that the duration and extent of magnetopause erosion play an important role in the spatiotemporal evolution of the plasma density distribution in the high-midlatitude ionosphere.

1. Introduction

The origin of geomagnetic storms and their impact on geospace has been studied by many in the past (Buonsanto, 1999; Elphinstone et al., 1996; Foster, 2008; Gonzalez et al., 1994; Prölss, 1995). While a large volume of literature describing the quiet and disturbed time behavior of the northern high latitudes is available, limited accessibility has contributed to sparse observational capability in the Southern Hemisphere. Nevertheless, a great deal of information has been collected using ground- and satellite-based observations, and a general understanding of the sequence of events that affects the high-latitude ionosphere during magnetically disturbed times has been achieved. The magnetic field that connects the high-latitude ionosphere to the magnetosphere allows the direct entry of particles of solar wind and magnetospheric origin into the polar ionosphere during quiet/disturbed times. The intensity of these processes enhances during periods of southward interplanetary magnetic field (IMF) which is a necessary condition for the magnetopause erosion (Aubry et al., 1970; Meng, 1970). Dayside reconnection results in the redistribution of magnetic flux and strengthening of the magnetospheric convection electric fields and field-aligned currents, leading to polar cap expansion and equatorward movement of the auroral oval (Le et al., 2016). The high-latitude ionosphere is also affected by the magnetic substorms (Elphinstone et al., 1996). The ionospheric convection and the dynamics of the polar cap during the growth and expansion phase of substorms agree well with the

Table 1
Geomagnetic Conditions on 17 March 2013 and 2015

Parameter	17 March 2013	17 March 2015
$F_{10.7}$ index	118	126
Commencement time	0600 UT	0445 UT
Minimum Dst	−130 nT	−223 nT
Duration of main phase	14 hr	17 hr
Peak AE	2,700 nT	2,200 nT

expanding/contracting polar cap (ECPC) paradigm (Clausen et al., 2013; Cowley & Lockwood, 1992; Lockwood & Cowley, 1992).

Energy input into the polar ionosphere in the form of particle precipitation, enhanced electric fields and currents, maximizes during the main phase of the storm and decreases during the recovery phase (Schunk & Nagy, 2000). Owing to the enhanced input of energy and momentum, numerous processes are triggered in the terrestrial ionosphere-thermosphere (IT) system that lead to either positive (enhancements in the plasma density) or negative (depletion of the plasma density) ionospheric storms in the polar ionosphere (Prölss, 1995). The negative ionospheric storms observed in the polar cap ionosphere are often associated with the composition disturbances originating from the enhanced joule heating of the polar atmosphere (Buonsanto, 1999; Prölss, 1995). The storm-induced joule heating of the polar atmosphere causes thermospheric expansion and large vertical flows (Prölss, 1995; Yeh et al., 1991). Consequently, the mean molecular mass of the thermosphere increases, and subsequently, the loss rates of the electrons is enhanced, resulting in a negative ionospheric storm. This depletion in the electron density is further amplified by the strong electric fields as they affect the ion reaction rates at high temperature (Rodger et al., 1992; St-Maurice & Torr, 1978).

However, when a geomagnetic storm is in progress, significant amounts of ionization (positive ionospheric storms) are observed in the polar cap ionosphere even during the winter time (Foster, 2008; Prölss, 1995; Shreedevi et al., 2019). The positive ionospheric storms over the polar cap ionosphere during the main phase of geomagnetic storms are often associated with soft particle precipitation and the formation of the storm-enhanced densities (SEDs)/tongue of ionization (TOI) (Correia et al., 2017; Mitchell et al., 2005; Shreedevi et al., 2019). The TOI is a large-scale structure of high-density plasma extending from the noontime cusp region across the polar cap in the noon-midnight direction. The SEDs that are formed at the lower latitudes through a complex interplay of storm time phenomena involving electric fields and neutral winds are known to be the source of the polar TOI (Foster, 2008; Lui, Wang, Burns, Yue, et al., 2016; Lui, Wang, Burns, Solomon, et al., 2016). Although the formation and evolution of ionospheric plasma structures like the SEDs and TOI have been studied for the past few years, there is not yet a single point of view regarding the mechanisms that drive the positive ionospheric storms in the high-midlatitudes. Because the degree of response of the ionosphere differs based on the state of the magnetosphere-ionosphere-thermosphere (MIT) system, which is partially controlled by factors like time of day, year, and solar cycle, there has been limited opportunity in the past to directly compare and contrast the causative mechanisms that lead to the generation of positive ionospheric storms. In this context, the St. Patrick's Day storms of 2013 and 2015 provide us an opportunity to understand how the IT system responds to two distinct space weather events of different intensities, occurring during similar background conditions (listed in Table 1) and nearly identical commencement times.

The St. Patrick's Day storm of 2015, the largest storm of the 24th solar cycle with Disturbance storm time (Dst) index reaching a minimum value of −238 nT, gathered immense interest among researchers and has been a subject of several investigations. Impact of an unusually intense magnetic storm on the near Earth space environment was the main focus of these studies (Astafyeva et al., 2015; Cherniak & Zakharenkova, 2016; Joshi et al., 2016; Le et al., 2016; Nava et al., 2016; Ramsingh et al., 2015; Tulasiram et al., 2015; Yadav et al., 2016; Wei, Yu, Ridley, et al. 2019; Wei, Yu, & He, 2019). Strong magnetopause erosion was shown to lead to significant changes in the magnetosphere during this severe geomagnetic storm (Le et al., 2016). Storm-induced changes in the neutral winds and composition played an important role in the spatial evolution of the polar TOI during this storm (Klimenko et al., 2019). Interhemispheric asymmetry in the storm response studied using SWARM satellite and GPS-TEC measurements (Cherniak & Zakharenkova, 2016) showed that the plasma density enhancements/irregularities associated with the SEDs/TOIs were more pronounced in the southern high-midlatitude ionosphere during 17 March 2015. Differences in the magnetic field geometry, changes in the O/N_2 ratio, and IMF B_y components were surmised to give rise to the hemispheric asymmetries in the ionospheric response (Astafyeva et al., 2015).

In the same solar cycle, another intense storm (minimum Dst ∼ −130 nT) occurred on the St. Patrick's Day of 2013. Large enhancements in magnetic field associated with substorm injections were observed using Van Allen Probes (Foster et al., 2013). The sharp fluctuating IMF B_z on this day led to a counter electrojet-like

Table 2
Geographic and Geomagnetic Coordinates of Stations Used in the Study

Station	Geo. Lat	Geo. Lon	Mag. Lat	Mag. Lon
Bharati	69.40°S	76.18°E	76.64°S	127.54°E
Davis	68.57°S	77.97°E	76.09°S	131.39°E

condition at the dip equator and resulted in a positive ionospheric storm impact throughout the equatorial and low-latitude ionospheric region (Shreedevi & Choudhary, 2017). Erosion of the plasmasphere, which took place under the action of the subauroral polarization streams (SAPS) electric field, gave rise to the formation of the TOI in the northern polar ionosphere (Foster et al., 2014). Images of the polar ionospheric electron density obtained through assimilating ground and Low Earth Orbit (LEO)-based TEC data revealed conjugate occurrences of SEDs/TOIs in both the Northern Hemisphere and Southern Hemisphere (Yue, Wan, et al. 2016). Using the coupled Thermosphere Ionosphere Electrodynamics General Circulation Model (TIEGCM), Dang et al. (2019) showed that the evolution of TOI in the northern polar region during the St. Patrick's Day storm of 2013 is strongly influenced by the plasma transport in the afternoon and morning sectors.

A comprehensive picture of the geospace system response to the St. Patrick's Day storm of 2013 and 2015 has been provided by Zhang et al. (2017). The storm-induced changes in the penetration electric field (Hairston et al., 2016), thermospheric neutral winds, and neutral composition (Klimenko et al., 2019; Yue, Wang, et al. 2016) and their impact on the high-midlatitude space weather during these storms were investigated in detail, but mostly as separate case studies. Only a few studies present a comparative analysis of the mechanisms that led to the ionospheric disturbances during these storms. For example, Verkhoglyadova et al. (2016) compared the responses in the TEC over the equatorial and northern midlatitude regions to show that the different responses during the St. Patrick's Day storms of 2013 and 2015 were driven by the differences in the solar wind drivers. Further, Dmitriev et al. (2017) used the Global Self-consistent Model of the Thermosphere, Ionosphere, and Protonosphere (GSM TIP) to predict the positive and negative ionospheric storms in the low-latitude and midlatitude regions during the St. Patrick's Day storms of 2013 and 2015. Their model could capture the negative ionospheric storms at midlatitudes, while the appearance of positive ionospheric storms especially during the recovery phase of the storm was unpredictable.

In this paper, we investigate in detail the relative impact of the St. Patrick's Day storms of 2013 and 2015 on the ionosphere over the southern polar cap region. Of particular interest are the positive ionospheric storms observed at the southern polar stations Bharati and Davis in the magnetic noon/midnight hours during both these storms, which suggest that the plasma density evolves in a similar manner during equivalent geophysical conditions. While the contributions of various storm time phenomena toward the formation of SEDs/TOI during these storms have been extensively studied, the role of external driving mechanisms in modifying the response of the polar ionosphere has not been paid attention. Hence, the main goal of the study is (1) to analyze in detail the mechanisms that lead to the generation of positive ionospheric storms over the southern polar cap region and (2) to understand the direct causative connection between the external driving forces and the ionospheric phenomena that lead to the similar yet distinct behavior of the plasma density over the southern polar cap region during the St. Patrick's Day storms of 2013 and 2015. The results of this study will provide insight into the solar wind control of the high-latitude ionospheric dynamics and will be useful in developing tools for prediction of space weather effects observed in the high-midlatitude ionosphere during geomagnetic storms. In the following, we describe our results in details and discuss their significance in developing understanding of the response of the Earth's polar ionospheric system to geomagnetic storms.

2. Data and Methodology

The response of the southern polar ionosphere to the St. Patrick's Day storm events of 2013 and 2015 is studied using GPS TEC measurements from two Antarctic research stations, Bharati and Davis. The geomagnetic and geographic coordinates of these stations are listed in Table 2. The receiver at Bharati is a Septentrio PolaRxS receiver, in which GPS TEC is estimated based on the L2-P and L1-P pseudoranges. The data acquisition software provides the binary 50-Hz raw correlation and phase data, which are further converted to Slant TEC (STEC) and scintillation indices. STEC obtained at an interval of 1-min is converted to vertical TEC (VTEC) using standard mapping function described by Smith et al. (2008). Although the receiver tracks satellites at elevation angles as low as 10°, we use only those satellite ray paths having an elevation angle greater than 30° and lock time greater than 240 s in the calculation of VTEC. The receiver at Bharati also provides the phase scintillation index (σ_ϕ) which is measured by the standard deviation of the
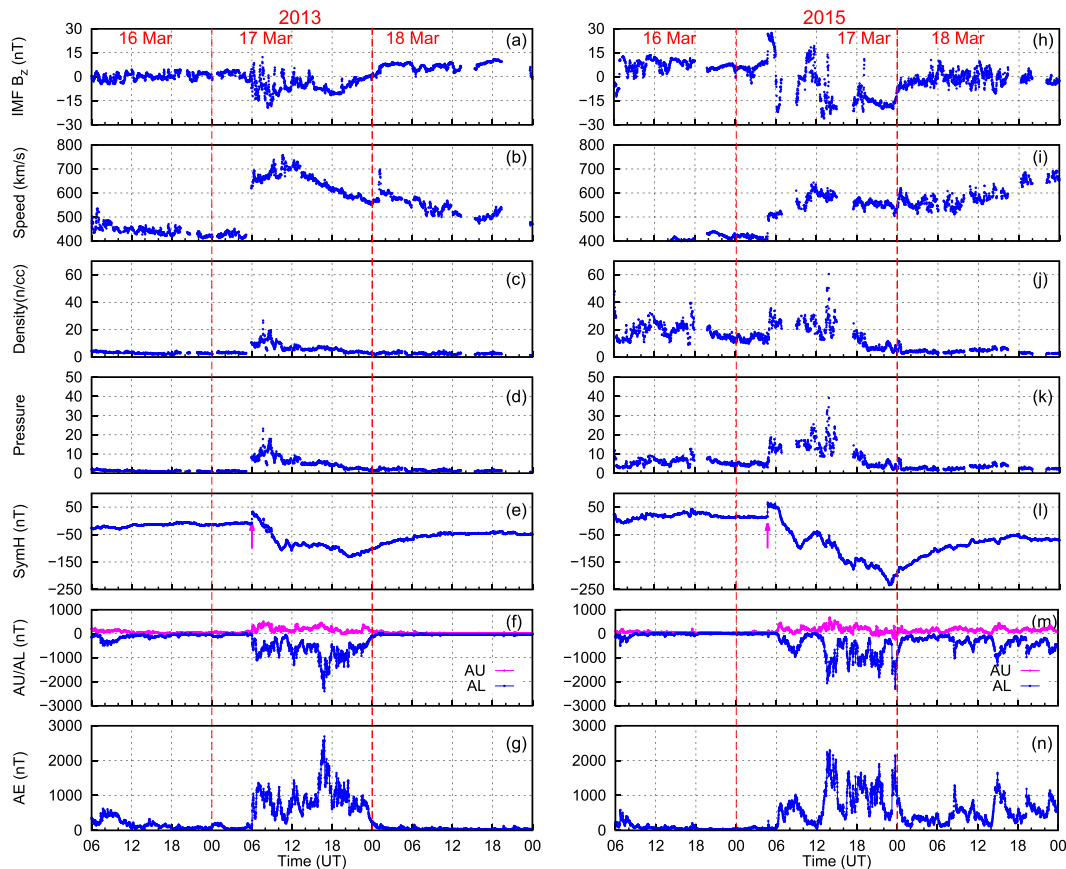
Figure 1. Geomagnetic conditions during 16–18 March 2013 and 16-18 March 2015: IMF B_z (panels a and h), solar wind (SW) speed (panels b and i), SW density (panels c and j), SW pressure (panels d and k), Sym-H (panels e and l), AU/AL (panels f and m), and AE indices (panels g and n). The pink arrows in panels (e) and (l) marks the time of SSC. The red vertical lines mark the change of day.

carrier phase averaged over intervals of 1, 3, 10, 30, and 60 s. The averaged values over 60-s σ_ϕ projected to the vertical as described by Spogli et al. (2009) are used in this study. The GPS TEC data from Davis station are downloaded from the IGS website (ftp://cddis.gsfc.nasa.gov) and consist of the standard RINEX files which are processed using GPS-TEC application (http://seemala.blogspot.com/) to obtain VTEC values. Daily Differential Code Biases (DCBs) for satellites and receivers are obtained from the CODE IGS Analysis Centre (http://ftp.aiub.unibe.ch/CODE/).

The solar wind, interplanetary, and geomagnetic parameters used to study the evolution of the geomagnetic storms are obtained from the Advanced Composition Explorer (ACE) satellite data and World Data Center, Kyoto, respectively, and are available on the CDAWeb (http://cdaweb.gsfc.nasa.gov). The changes in the thermospheric composition on 17 March 2013 and 17 March 2015 are studied using the O/N_2 maps obtained from Global Ultraviolet Imager (GUVI)/Thermosphere Ionosphere Mesosphere Energetics and Dynamics (TIMED) measurements. A detailed description of the GUVI instrument and the data products are found in Paxton (2005) and Christensen (2003). Measurements from the polar orbiting DMSP satellite are examined as it follows a sun-synchronous dawn-dusk orbit at an altitude of 840 km and therefore is able to provide insight into the response of the topside polar ionosphere to geomagnetic storms. In situ measurements of particle fluxes, plasma density, and cross-track velocity components by DMSP satellites are used to study the signatures of particle precipitation, SAPS and the TOI. The auroral images of the southern polar ionosphere provided by the Special Sensor Ultraviolet Spectral Imager (SSUSI) instrument onboard DMSP satellites are used to understand the response of the auroral ionosphere to the storm time energy input. SSUSI measures the far ultraviolet (FUV) auroral and airglow emissions in five channels (1,216, 1,304, 1,356 Å, Lyman-Birge-Hopfield short [LBHS], and Lyman-Birge-Hopfield long [LBHL]) (Paxton et al., 1992a,

1992b). In the present study, we have used the emissions derived from the N_2 LBHS channel (N_2 emissions in the 1,400- to 1,500-Å range).

GPS TEC maps generated using the TEC data from the Madrigal database (http://madrigal.haystack.mit. edu/madrigal/) are used to understand the variations in the TEC in the Southern Hemisphere. The GPS TEC maps are overlaid with the ionospheric convection maps obtained using the SuperDARN Auroral Radar Network (SuperDARN) data (Chisham et al., 2007). Such a combination allows for comparison of the TEC variations along the path of convection (Rideout & Coster, 2006; Thomas et al., 2013).

The signatures of the prompt penetration electric field (PPEF) are deduced from the changes in the equatorial electric field. The equatorial electrojet (EEJ) strength which is a good proxy for the zonal electric field (Rastogi & Klobuchar, 1990) is derived using the standard procedure of subtracting the magnetic field perturbations at an off equatorial station Alibag (18.64°N, 72.91°E, dip latitude 10.4°SN) from that of an equatorial station Tirunelveli (8.3°N, 77.8°E, dip latitude 0.24°S) (Anderson et al., 2002).

3. Geomagnetic Conditions During the Storm Events

Figure 1 shows the solar wind and geomagnetic conditions during 16–18 March 2013. The sudden enhancement in the solar wind speed, density, and pressure (Figures 1b–1d) led to the sharp increase in SymH index (Figure 1e) at 0600 UT and marked the sudden storm commencement (SSC) of the geomagnetic storm on 17 March 2013. The main phase of the storm began with the southward turning of IMF B_z immediately after the SSC at 0600 UT. The IMF B_z on 17 March 2013 was mostly fluctuating in nature as it oscillated between southward and northward directions with a period of ~1.5 hr till 1400 UT. Later, it remained southward for ~0600 hr and then gradually turned northward. The geomagnetic storm is seen to have two minima with Sym-H reaching a first minima of approximately −100 nT at ~1,030 UT and a second minima of approximately −130 nT at ~2030 UT. A slow recovery phase is seen to follow after 2030 UT.

Similarly, the solar wind and geomagnetic conditions during 16–18 March 2015 are depicted in Figures 1g–1n. The geomagnetic storm on 17 March 2015 also commenced with an initial increase of IMF B_z at 0445 UT as can be seen in Figure 1l. The IMF B_z turned southward at ~0530 UT and remained southward till ~2400 UT except for a brief period of about 2 hr between ~1000 and ~1200 UT when it had a northward polarity. The Sym-H index reached a first minima of approximately −100 nT at ~0930 UT but later turned positive when IMF B_z was northward between 1000 and 1200 UT on 17 March 2015. Post 1200 UT, as the IMF B_z turned southward, there was a step like increase in the solar wind speed followed by a rise in the solar wind pressure and density (~40 nPa and 60 cm^{-3}, respectively). The sudden rise in the solar wind speed, pressure, and density was followed by a period when the Sym-H index reached a second minima of approximately −223 nT. The recovery phase of the geomagnetic storm is seen to occur after 2300 UT.

Even though the SSC during the geomagnetic storm on 17 March 2015 took place an hour before the SSC on 17 March 2013, the onset of the main phase of both the storms was at 0600 UT. The variation of Sym-H index is also quite similar in both the cases till they attain the first minimum of approximately −100 nT. The solar wind density and pressure enhancements were larger and had longer duration on 17 March 2015, as compared to those on 17 March 2013. The main phase of the geomagnetic storm on 17 March 2013 lasted for ~14 hr, while that on 17 March 2015 lasted for ~17 hr. During the entire duration of the main phase, the Auroral Electrojet (AE) index remained high indicating strong currents and intense heating taking place at the polar latitudes. The Electrojet lower (AL) index which is an indicator of the auroral electrojet activity implies that a number of substorms were triggered during the main phase of these storms. How the southern polar ionosphere responded to the aforementioned similarities and differences in the solar wind and geomagnetic conditions during the St. Patrick's Day storms of 2013 and 2015 is discussed in the subsequent sections.

4. Response of the Southern Polar Ionosphere

To understand the plasma density variations in the southern polar ionosphere during 17 March 2013 and 17 March 2015, we examined the variation of TEC at the Antarctic stations, Bharati and Davis on these two days. The diurnal variation of TEC on 17 March 2013 at Bharati and Davis is shown in Figures 2a and 2c, respectively. The 1-σ standard deviation of five quietest days of the month at the stations is highlighted by
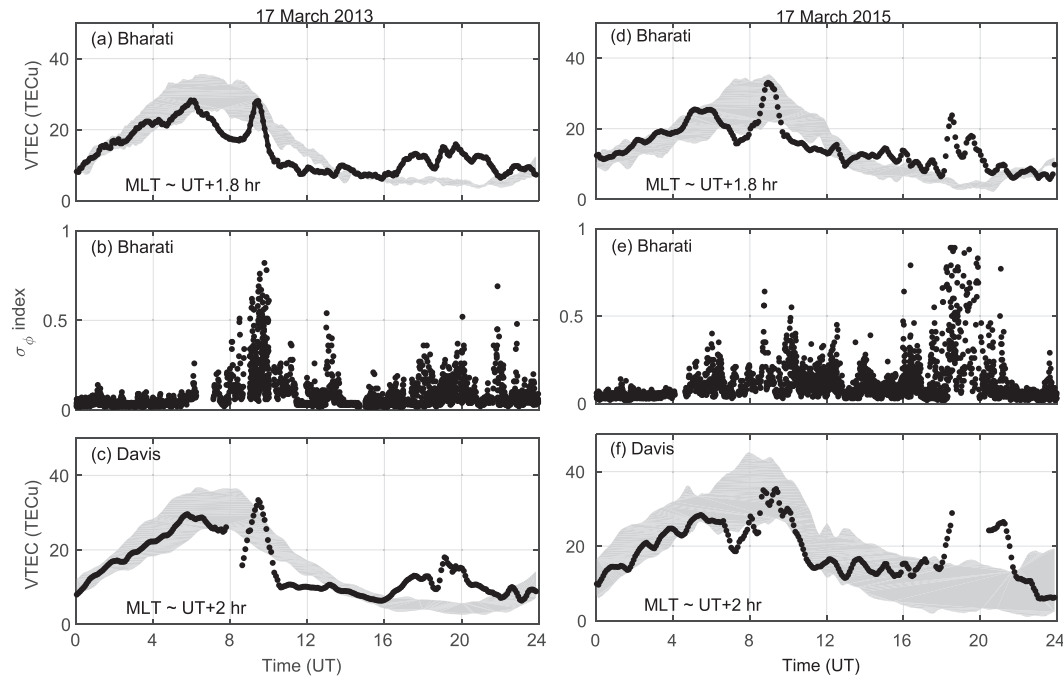
Figure 2. Panels (a) and (b) represent the diurnal variation of TEC and σ_ϕ index, respectively, at Bharati on 17 March 2013, while panel (c) represent the diurnal variation of TEC at Davis station on 17 March 2013. Similarly, panels (d) and (e) represent the diurnal variation of TEC and σ_ϕ index, respectively at Bharati on 17 March 2015, while panel (f) represents the diurnal variation of TEC at Davis station on 17 March 2015. The black curve in panels (a), (c), (d), and (f) represent the variation in TEC respectively on the day of the storm and the gray shade represents the quiet day standard deviation.

the gray shading. The immediate effect of the commencement of the geomagnetic storm on this day can be seen as a sudden decrease in the TEC starting at 0600 UT at both the stations. A striking feature in Figures 2a and 2c is the enhancements in TEC at two distinct times at both Bharati and Davis stations. The first sharp enhancement in TEC is observed at around 1000 UT during the daytime. Though the TEC values during this time remained close to the 1-σ standard deviation, the sudden surge in the magnitude of TEC can be easily identified from the Figure 2. A second enhancement in the TEC of ~10 TECu appeared during 1600–2200 UT at Bharati and Davis which is significantly above the upper bound of 1-σ deviation of the mean monthly TEC. These abrupt surges in TEC during the two time periods coincided with enhanced levels of phase scintillation activity at Bharati in the local magnetic noon as well in the magnetic midnight as shown in Figure 2b. It is known that the phase scintillations in the GPS signals indicate fluctuations in the plasma density of the ionosphere (Wernik et al., 2007). A larger magnitude of σ_ϕ indicates greater fluctuations in the plasma density. We may note that the σ_ϕ in Figure 2b increased from close to ~0.3 to ~0.8 during the period when the first surge in TEC (around 1000 UT) was observed. A similar albeit of moderate intensity phase fluctuations in the GPS radio signals can be seen during the second surge of the TEC (~1600–2200 UT) as well. The increase in the TEC and phase fluctuations complement each other. An interesting thing to note is the timing of the increase in the TEC. While the first increase in the TEC is seen at around 1000 UT (1530 LT), a post solar local noon period; the second enhancement at 2000 UT (0130 LT) corresponds to the post solar local midnight.

Similarly, Figures 2d and 2f present the diurnal variation in the TEC on 17 March 2015 at Bharati and Davis respectively. 1-σ standard deviation in the TEC at these stations is shown by gray shade. The phase scintillation index (σ_ϕ) for the GPS radio signals at Bharati is shown in Figure 2e. Like the case on 17 March 2013, a sudden decrease in the TEC is observed at the two stations on 17 March 2015 following the commencement of geomagnetic storm at ~0545 UT. The TEC at Bharati and Davis starts to increase later at 0700 UT. It is to be noted that large enhancements in TEC (~20 TECu) are observed around 1900 UT at Bharati and Davis similar to those observed on 17 March 2013. The magnitude of the TEC at Bharati during this period is very high, that is, ~20 TECu compared to ~5 TECu, which is the monthly average during this time of a day in
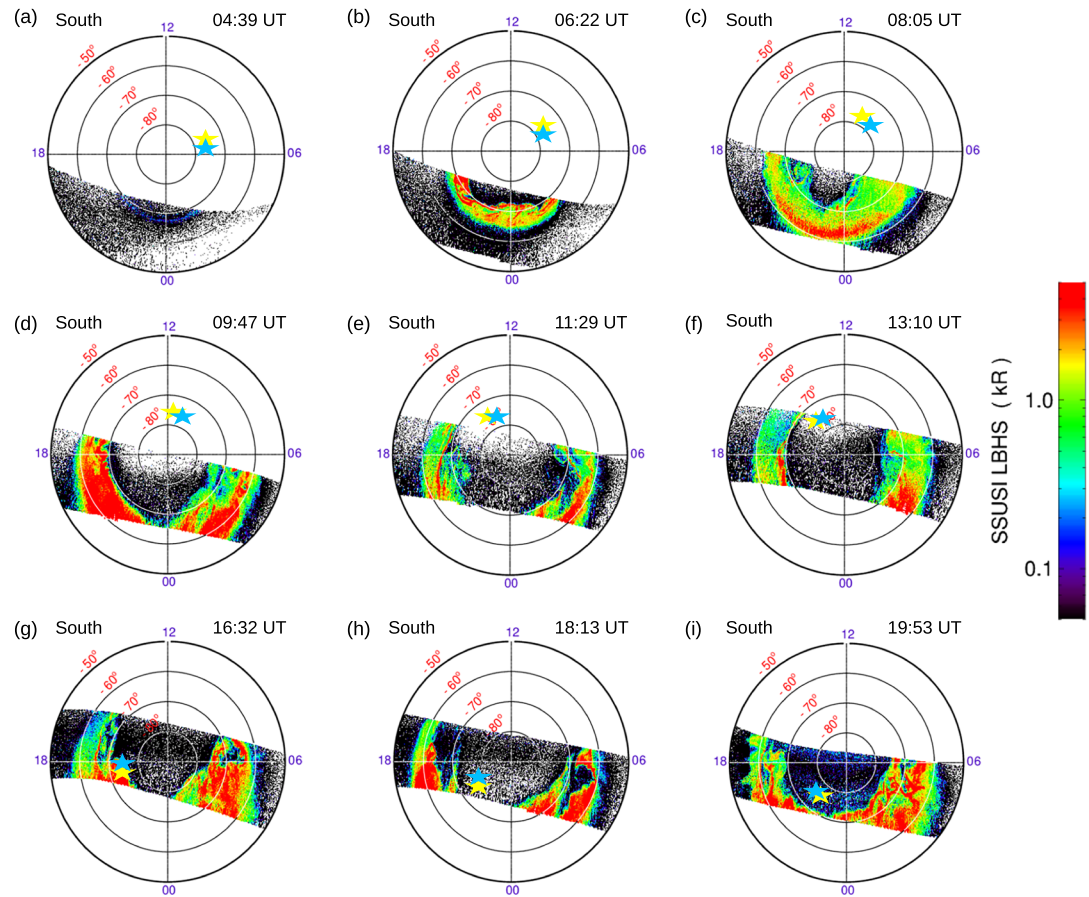
Figure 3. Panels (a)–(i) show the auroral emissions derived from the N_2 LBHS channel at different times on 17 March 2013. The approximate locations of the stations Bharati and Davis are marked using yellow and blue color, respectively.

March. Such a huge increase in the plasma concentration happens during the time when the station is located in the night sector, quite bereft on solar radiation, which is an important source of plasma in the Earth's ionosphere. This increase in TEC at Bharati is also seen to coexist with higher values of σ_ϕ index (~0.9) indicating high scintillation activity. A comparatively smaller enhancement in the TEC that remains well below the upper bound of 1-σ can be seen at ~0900 UT at both the stations on 17 March 2015.

Studies have shown that the evolution of plasma density at a polar cusp station depends on the position of the station with respect to the polar cap/auroral oval (Knudsen, 1974; Shreedevi et al., 2019). To understand the response of the auroral ionosphere to the storm time energy input and illustrate the changes in the size and location of the auroral oval/polar cap with respect to the location of the stations, Bharati and Davis, we use the auroral images of the southern polar ionosphere during the St. Patrick's Day storm events. The auroral images obtained from the SSUSI instrument onboard DMSP F16 satellite at selected times are shown in Figures 3 and 4. The approximate locations of Bharati and Davis stations are marked on Figures 3 and 4 using yellow and blue colors, respectively. Unfortunately, the DMSP passes in the Southern Hemisphere mostly span the nightside region, and hence, we cannot use it to point out the changes in the dayside auroral ionosphere. However, it can be inferred from Figure 3 that during the time of SSC at ~0600 UT on both the days, Bharati (shown in blue) and Davis (shown in yellow) are located in the vicinity of the auroral oval. On 17 March 2013, at 0622 UT, when the IMF is largely southward, one can see a large equatorward expansion of the auroral oval with a significant enhancement in the brightness of the aurora. At later times (see Figures 3c–3i), the auroral oval can be seen to undergo several changes including the equatorward/poleward expansion and variation in the brightness of the aurora. It is to be noted that the stations, Bharati and Davis located in the polar cap in the magnetic noon-to-midnight sector, lie in the vicinity of regions of strong auroral emissions on 17 March 2013.
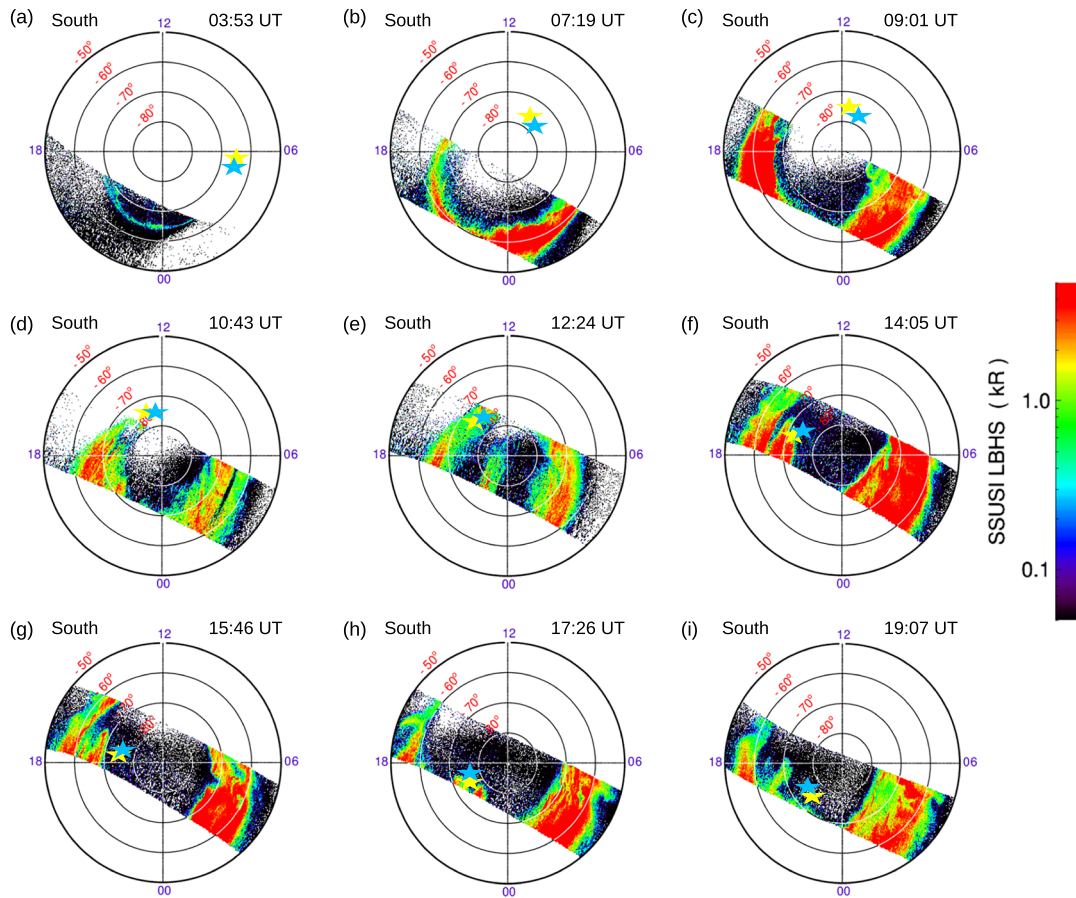
Figure 4. Panels (a)–(i) show the auroral emissions derived from the N_2 LBHS channel at different times on 17 March 2015. The approximate locations of the stations Bharati and Davis are marked using yellow and blue color, respectively.

During the early main phase of the storm on 17 March 2015 also, there are large expansions in the polar cap and the auroral oval in response to the southward turning of IMF as evident from Figures 4b and 4c. It can be seen that by 0901 UT (Figure 4c), the equatorward boundary of the auroral oval reached ~52°S MLAT. More intense emissions along with large equatorward expansion of the auroral oval in response to the second southward turning of the IMF at ~1400 UT can be seen from Figure 4. The auroral activity on 17 March 2015 was stronger compared to that on 17 March 2013 with notable features like the intense emissions throughout the main phase of the storm and complex flows in the polar cap as suggested by the appearance of the sun-aligned arcs (Valladares et al., 1994). It is to be noted here that during the most part of the storm duration on 17 March 2015, the stations are located in regions of strong emissions which could be a source region for generation of ionospheric irregularities (Moen et al., 2013).

The ionospheric TEC is known to be primarily influenced by the storm time electric fields in the topside ionosphere, while the composition changes brought about by neutral winds largely affect the bottom side ionosphere (Lui, Wang, Burns, Yue, et al. 2016). Information about the changes in the topside ionospheric parameters during the St. Patrick's Day storm events of 2013 and 2015 is obtained from the DMSP satellites. Figures 5a–5e show the energy spectrograms of electrons and ions, ion density, and horizontal and vertical velocity in the Southern Hemisphere on 17 March 2013 measured by the DMSP F16 satellite at 840 km during a pass at around 0930 UT. The energy spectrograms show the presence of large electron and ion energy fluxes suggesting enhanced particle precipitation into the southern high-latitude ionosphere during this period. The electron and ion precipitation boundaries are observed at ~56°S MLAT (is marked using a black line in Figure 5). The ion flux calculated as the product of the density and the cross-track velocity is shown in Figure 5e. One can see the presence of enhanced sunward velocities (greater than ~2 km/s) and vertical velocities in the subauroral region. This region of enhanced velocities is also colocated with regions of large
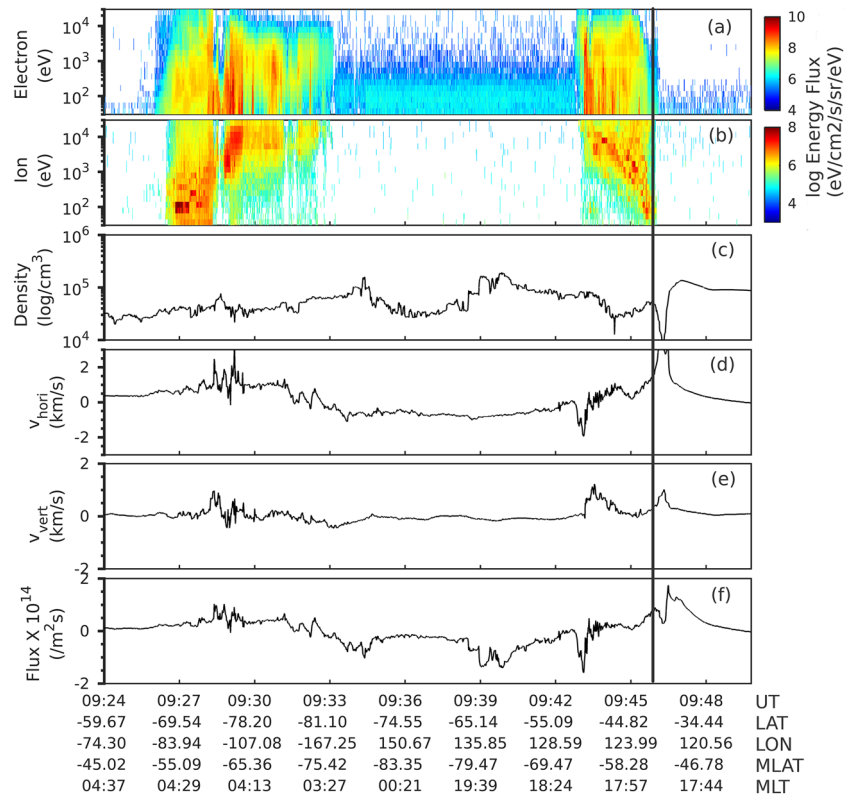
Figure 5. DMSP F16 observations during a pass in the Southern Hemisphere on 17 March 2013: Panels (a) and (b) show the energy spectrograms of electrons and ions in log scale. Panels (c) and (d) represent the density and cross-track velocity in horizontal and vertical directions, respectively. The ion flux calculated as a product of density and cross-track velocity is shown in panel (f). The electron and ion precipitation boundary located equatorward of the auroral oval at ∼56°S MLAT is marked using the black line.

sunward flux (∼1.5×10^{14} m^2/s). This is a signature of the SAPS electric field (Foster & Burch, 2002) that are known to develop in the subauroral regions to achieve current continuity by closing the region-1 FACs and the region-2 FACs (Yeh et al., 1991). During this period, large antisunward velocities (∼1 km/s) and fluxes are also observed in the southern polar cap as evident from Figures 5d and 5f, respectively. This period (around ∼0930 UT) is also marked by an increase in plasma density in the polar cap region (as shown in Figure 5c).

The energy spectrograms of electrons and ions, ion density, and horizontal and vertical velocity in the Southern Hemisphere on 17 March 2015 as measured by the DMSP F17 satellite during a pass are shown in Figures 6a–6e. The energy spectrograms of electrons and ions show enhanced particle precipitation in the auroral as well as polar cap regions of the Southern Hemisphere at around 0900 UT. The electron and ion precipitation boundaries are at ∼51°S MLAT which is ∼5° lower than what was observed on 17 March 2013. Large vertical and sunward flow velocities of upto ∼2 km/s are observed at latitudes equatorward of the auroral oval on this day. Large fluxes of magnitude ∼1.5×10^{14} m^2/s are seen to flow in the sunward direction at these latitudes which as described earlier is known to be the case under the action of the SAPS electric field. The presence of large antisunward velocities (2 km/s) and fluxes (of magnitude -2×10^{14} m^2/s) in the polar cap region is evident from Figure 6. The plasma density in the polar cap region is seen to be high at ∼0900 UT on this day also. It is to be noted here that the first enhancement in TEC at the southern polar stations Bharati and Davis was also centered about ∼0900 UT on 17 March 2013 as well as 17 March 2015.

In order to examine if the variations in the TEC were caused by thermospheric composition changes in the southern high-latitude regions, we present O/N_2 maps obtained from the GUVI instrument on board the TIMED satellite. The O/N_2 ratio on 17 March 2013 and 17 March 2015 are shown in Figures 7b and 7d respectively along with the quiet day variations in the respective months (Figures 7a and 7c). One can see
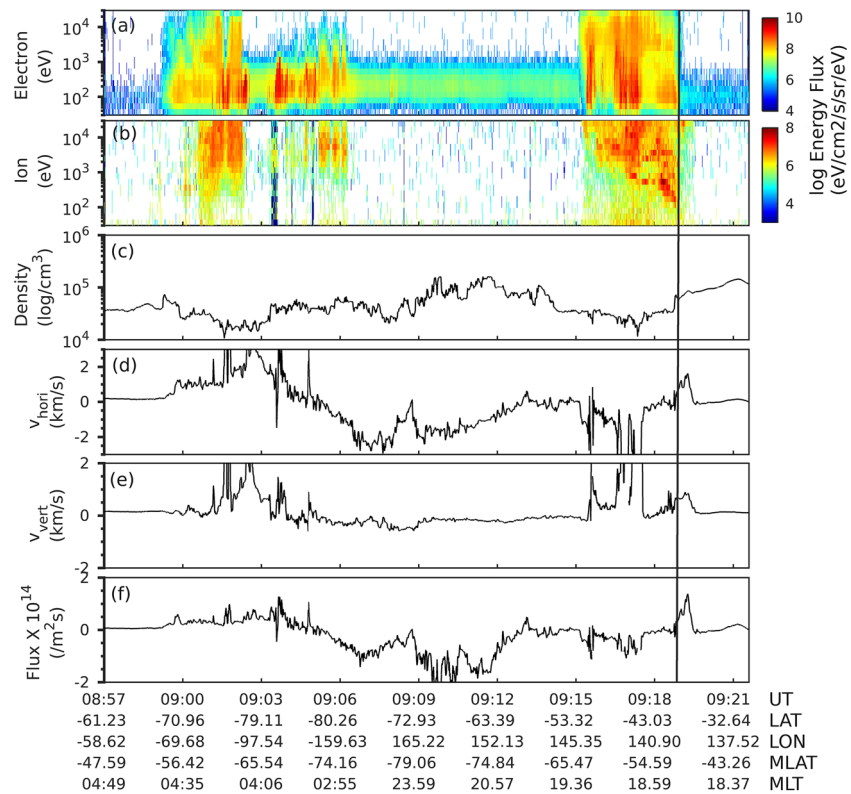
Figure 6. DMSP F17 observations during a pass in the Southern Hemisphere on 17 March 2015: Panels (a) and (b) show the energy spectrograms of electrons and ions in log scale. Panels (c) and (d) represent the density and cross-track velocity in horizontal and vertical directions, respectively. The ion flux calculated as a product of density and cross-track velocity is shown in panel (f). The electron and ion precipitation boundary that is located equatorward of the auroral oval at ~51°S MLAT is marked using the black line.

a reduction in the O/N_2 ratio over the high-latitude regions on 17 March 2013 in comparison with the O/N_2 variation on a quiet day, that is, 14 March 2013. Similarly, there is a large reduction in the O/N_2 ratio over the southern high-latitude regions on 17 March 2015 as compared to that on 14 March 2015. This clearly indicates the presence of composition disturbances at the high-latitude regions on these days. Studies have shown that the enhancement in the O/N_2 ratio over the low and equatorial regions during storm time can lead to a positive ionospheric storm while a reduction in the O/N_2 ratio over the high latitudes can bring about a negative ionospheric storm (Prölss, 1995; Shreedevi et al., 2016). Except for the reduction in the TEC for a short period during the initial phase of the storms, we find that the TEC at Bharati and Davis exhibit enhancements on 17 March 2013 as well as 17 March 2015.

5. Plausible Reasons for the Enhancements in the TEC

As described in the previous sections, during the St. Patrick's Day storms of 2013 and 2015, the TEC at the southern polar stations Bharati and Davis evolved in a similar fashion with a reduction in the TEC (negative ionospheric storm) during the early main phase followed by enhancements in the TEC (positive ionospheric storm) at two distinct time zones during the main phase. This feature is discernible over Bharati and Davis during both the events. The midnight enhancement in TEC and phase scintillations on 17 March 2015 were substantially larger in magnitude as compared to that observed on 17 March 2013. During both the events, the first increase in the TEC started at around 0900 UT, that is, ~3hr after the SSC and peaked at ~1000 UT. During this time, Bharati and Davis are located in the magnetic cusp region. The second enhancement, on the other hand, appeared around 1900 UT (in the magnetic midnight sector) when the stations are located in the polar cap. This is the time when the stations remain completely in darkness and so the contribution from
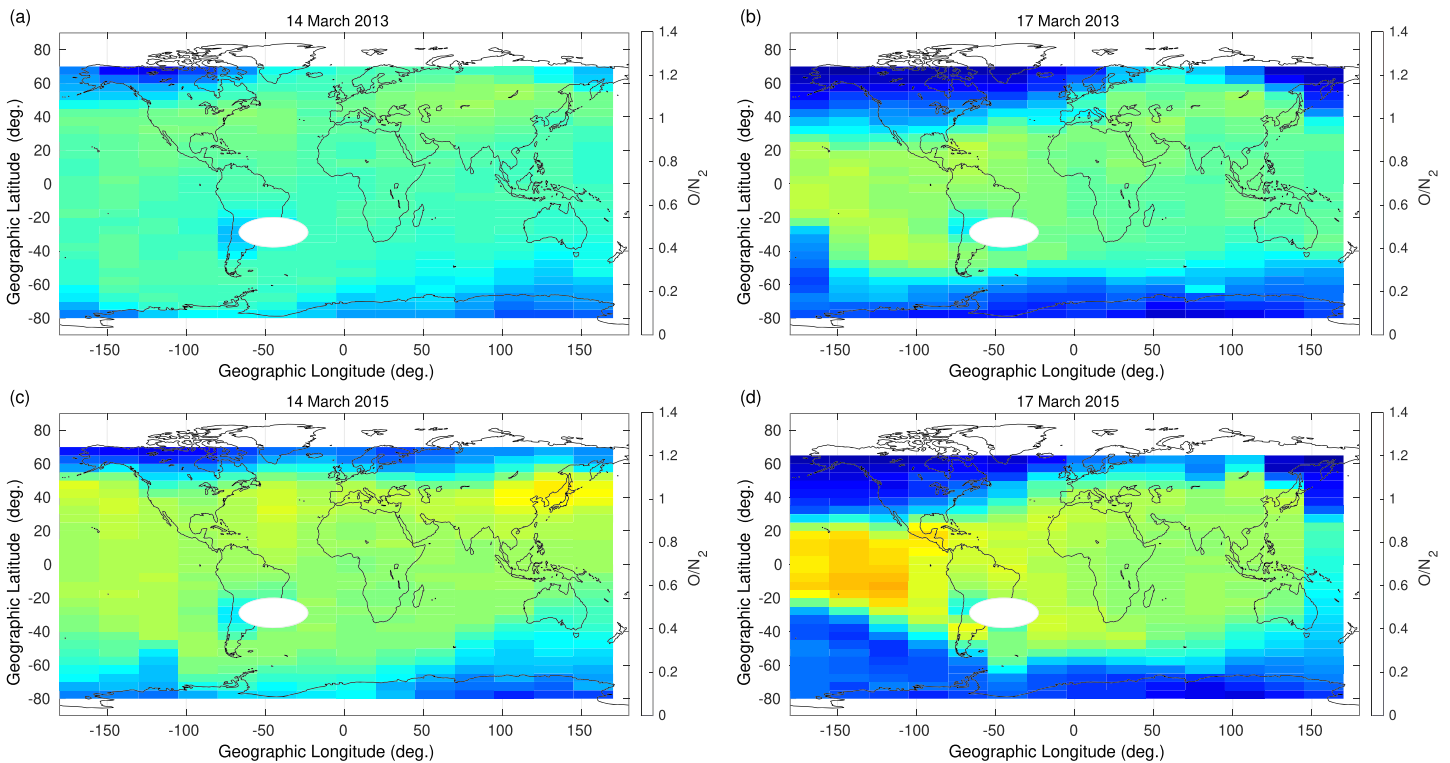
Figure 7. Global maps of O/N_2 ratio obtained from the TIMED/GUVI satellite measurements to show the composition changes in the thermosphere: Panels (a) and (c) show the O/N_2 ratio on 14 March 2013 and 14 March 2015 which are representative quiet days in the respective months. Panels (b) and (d) show the O/N_2 ratio on the St. Patrick's Day storms of 2013 and 2015, respectively. The blank oval represents the region of South Atlantic Anomaly.

the solar photo ionization toward enhancement of the nighttime TEC is absent. Therefore, the surges in TEC (~10 TECu on 17 March 2013 and 20 TECu on 17 March 2015) could be due to contributions from any mechanisms other than direct photo ionization.

Nighttime enhancements in the plasma density that appear in the polar cap ionosphere during geomagnetic storms are often associated with the formation of the polar TOI (Foster et al., 2005; Shreedevi et al., 2019). In order to confirm if the passage of the TOI led to the enhancement in the TEC at Bharati and Davis stations, the GPS TEC maps of the southern polar ionosphere at selected times (1600–2200 UT) on 17 March 2013 are shown in Figures 8a–8f. The approximate location of Bharati and Davis stations is marked on the GPS TEC maps using pink and black stars, respectively. The SuperDARN convection pattern are overlaid on the TEC maps to understand the TEC variations along the path of ionospheric convection. No trace of the TOI formation is seen in the TEC maps at 1600 UT on 17 March 2013. At 1630 UT, plasma of high density can be seen to form around the noon time cusp region (see Figure 8b). At later times, that is, during 1730–1900 UT (Figures 8c–8e), the plasma of higher density (~12–20 TECu) associated with the TOI is seen at the location of Bharati and Davis. The TOI is seen to vanish by about 2200 UT as the IMF turns northward and the ionospheric convection weakens on 17 March 2013. Likewise, Figure 9 shows the evolution of TEC and convection pattern over the southern polar ionosphere during 1600–2200 UT on 17 March 2015. A region of enhanced TEC (>20 TECu) can be seen to form at the magnetic noon during 1700–1730 UT on 17 March 2015. The extension of the TOI into the polar cap along the path of convection is evident from Figures 9b–9f. At 1830 and 1930 UT, patches of enhanced TEC can be seen at locations of the stations, Bharati and Davis. These evidences show that during the storms of 17 March 2013 and 17 March 2015, Bharati and Davis were in the vicinity of a stream of high-density plasma flowing in the antisunward direction across these stations located in the polar cap in the magnetic midnight sector. The midnight enhancement in the TEC at these stations on 17 March 2013 and 17 March 2015 is hence associated with the TOI. However, the decrease in the O/N_2 ratio at the southern high latitudes during both the storms (see Figure 7) would suggest an increase in the loss rates and a decrease in the plasma density threat, which
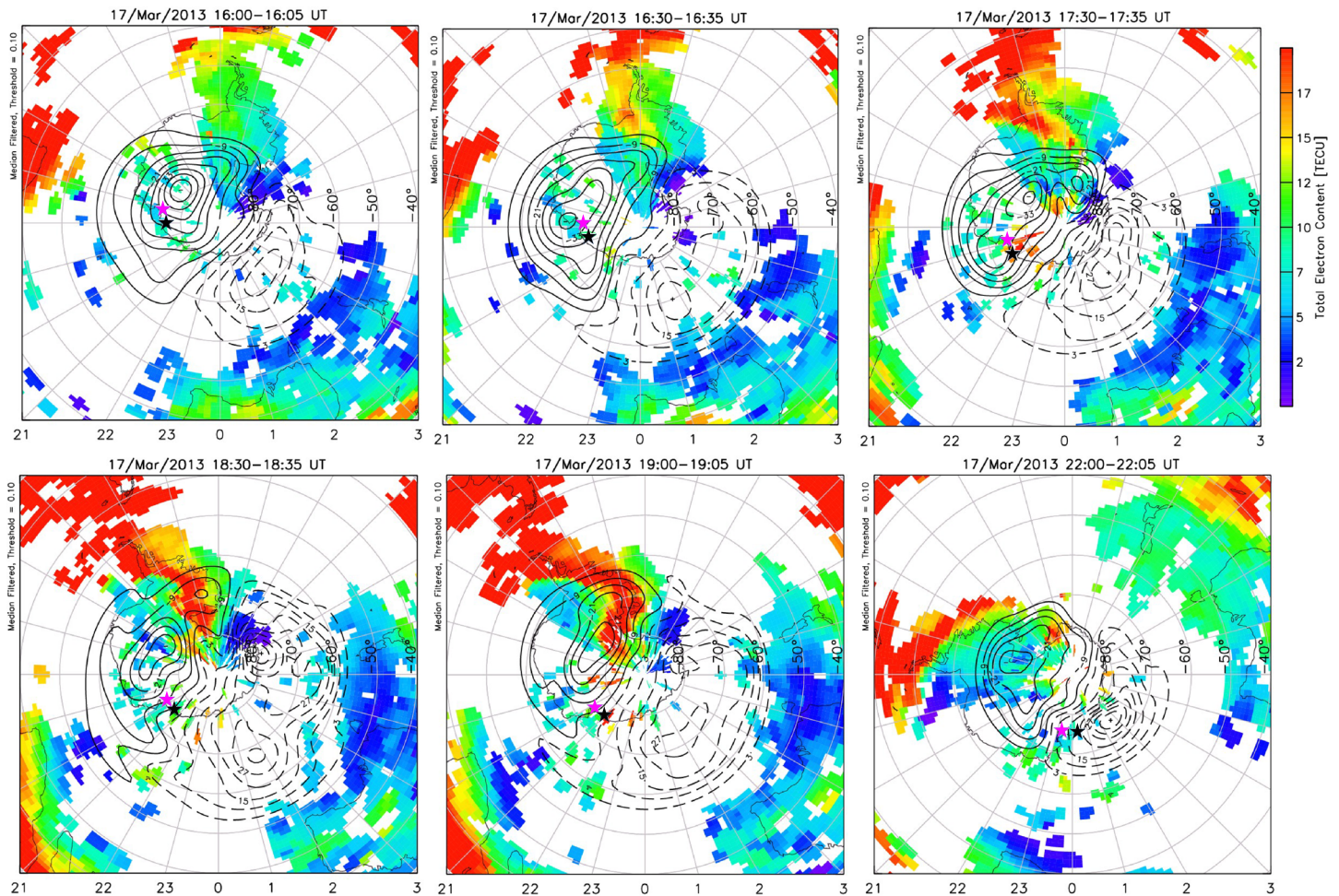
Figure 8. Panels (a)–(f) show the TEC in the Southern Hemisphere at selected times (1600 UT, 1630 UT, 1730 UT, 1830 UT, 1900 UT, and 2200 UT) on 17 March 2013. The SuperDARN convection pattern is overlaid on the TEC maps to show the TEC variation along the path of convection. The location of Bharati and Davis stations are marked on the maps using pink and black stars, respectively.

is contrary to what is observed. Therefore, the contribution to the TEC enhancements at Bharati and Davis cannot come from the neutral composition disturbances but rather from the topside ionosphere. This is supported by a recent study of Klimenko et al. (2019), who using the GSM TIP model showed that the neutral composition disturbances during 17 March 2015 storm have a stronger influence in the bottomside ionosphere than at altitudes above the F region.

Unfortunately, due to the sparse coverage of the GPS receivers in the eastern part of Antarctica, we cannot fully trace the formation of the TOI using the TEC maps during the early main phases of the St. Patrick's Day storms of 2013 and 2015, and so we do not present the GPS TEC maps of the southern polar ionosphere during 0900–1000 UT here. However, the presence of enhanced particle precipitation, antisunward fluxes, and high ion density in the polar cap region at around 0900 UT during both the storm events is confirmed by the DMSP observations. This provides clear evidences for (1) enhanced cusp precipitation of low energy electrons into the ionosphere that could lead to enhancement in the plasma density and (2) the transport of plasma into the noontime cusp regions leading to enhancement in the TEC. Since the stations are located in the vicinity of the cusp region during magnetic noon, they may lie in the path of the TOI. Hence, the daytime positive storms at Bharati and Davis in the magnetic noon sector appear as the SED plumes generated at midlatitudes enter the cusp region, while the positive ionospheric storms observed during the nighttime are the TOI resulting from the SED plumes that entered the southern polar cap through the cusp region. Previously, Yue, Wan, et al. (2016) identified the SED/TOI structures during the early main phase (~0900 UT) and the main phase (~1875 UT) in the Northern Hemisphere on 17 March 2013 from images of the
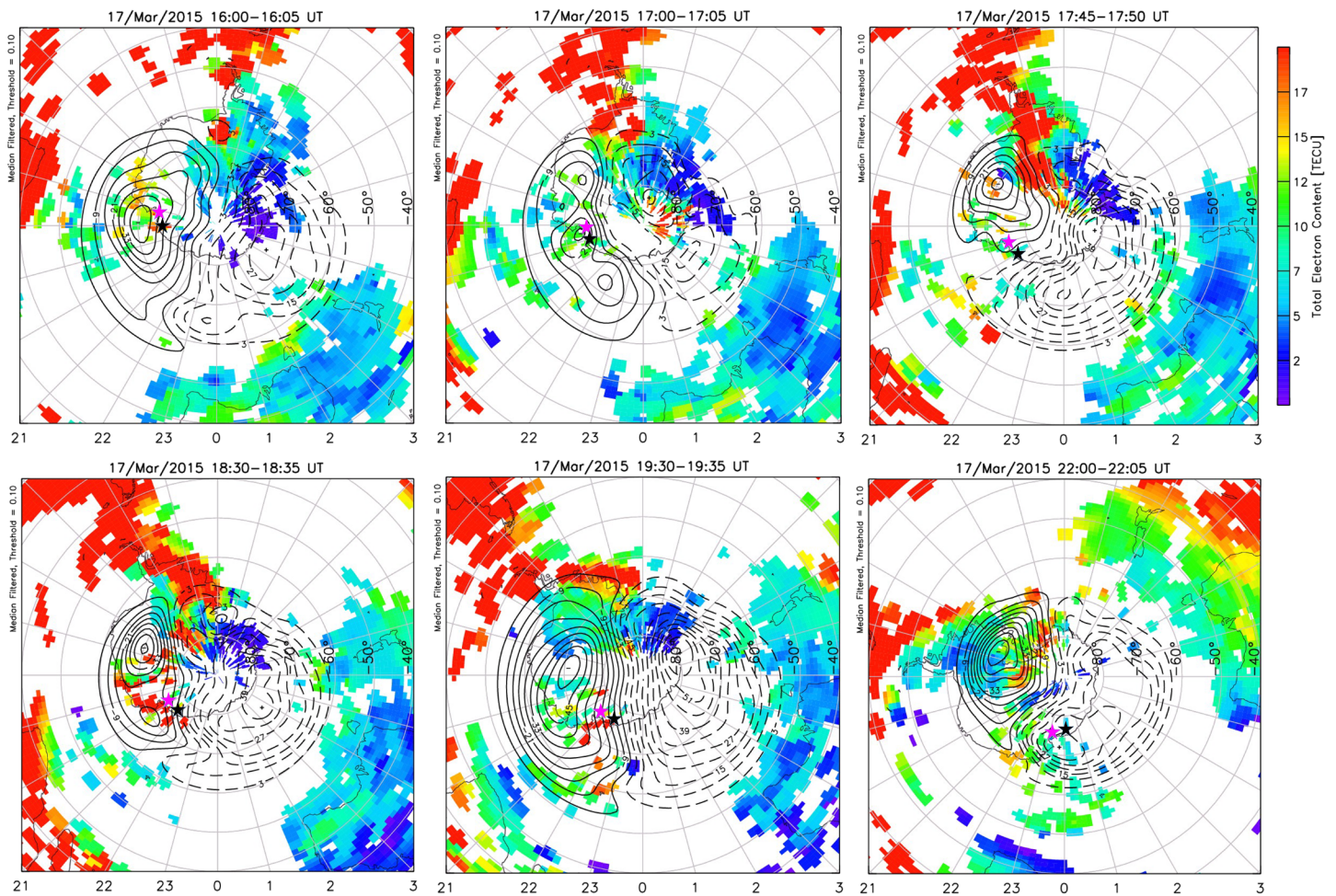
Figure 9. Panels (a)–(f) show the TEC in the Southern Hemisphere at selected times (1600, 1700, 1745, 1830, 1930, and 2200 UT) on 17 March 2015. The SuperDARN convection pattern is overlaid on the TEC maps to show the TEC variation along the path of convection. The location of Bharati and Davis stations is marked on the maps using pink and black stars, respectively.

global ionospheric electron density obtained through assimilating ground and LEO-based TEC data. They also suggested the occurrence of SEDs/TOI in the Southern Hemisphere during these periods owing to the magnetically conjugate expansion of the convection electric field which is well in agreement with our results. Similarly, signatures of the polar TOI have been detected in the measurements of the SWARM electron density and GPS TEC in the Southern Hemisphere during the St. Patrick's Day storm of 2015 (Cherniak & Zakharenkova, 2016; Klimenko et al., 2019).

The presence of intense phase scintillation activity at Bharati is observed during periods of abrupt enhancements in TEC at around ~1000 UT, that is, when the station lies in the vicinity of the cusp and at ~2000 UT when the station lies in the polar cap. Such strong scintillations are associated with the gradients in the TEC which could arise due to intense particle precipitation, complex flows, and strong ionospheric convection (Aarons, 1997; Mitchell et al., 2005), the presence of which are confirmed by DMSP observations described in the previous sections. As the GPS signal traverses through regions of irregularities, they undergo phase fluctuations. Although phase scintillations were present throughout the main phase of the storm on 17 March 2013 and 17 March 2015, they were especially strong in the magnetic midnight sector on 17 March 2015. The auroral images clearly suggest the presence of large plasma gradients and instabilities at the location of the station (in the polar cap) on 17 March 2015 (see Figure 4). Further, the GPS TEC maps of the period 1700–1900 UT on 17 March 2015 clearly show patches of enhanced TEC colocated with regions of strong convection. The TOI which is a continuous flow of high-density plasma may also break into patches while convecting through the polar cap (Sojka et al., 1993) and form the source of ionospheric irregularities
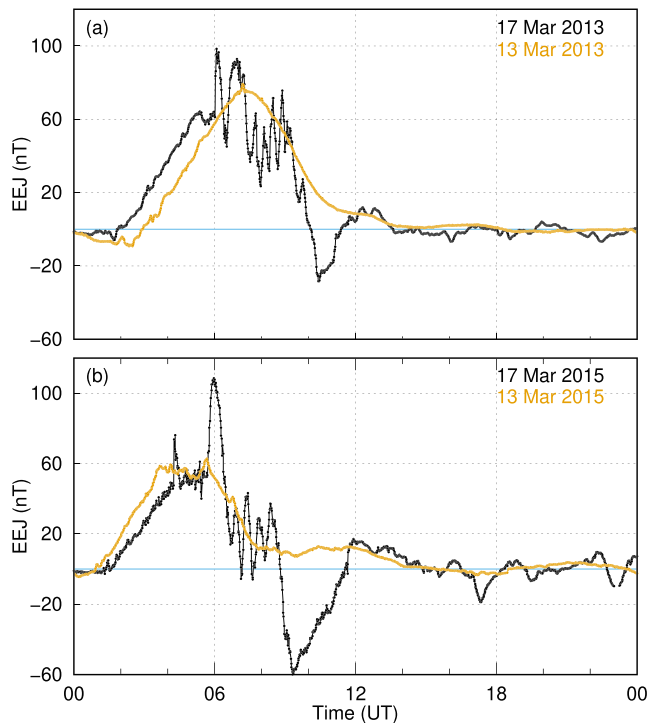
Figure 10. Panels (a) and (b) represent the variation of the equatorial electrojet (EEJ) strength on 17 March 2013 and 17 March 2015, respectively. The brown line in panels (a) and (b) represents the variation of EEJ strength on a quiet day in the month of March in the respective years.

which in turn gives rise to scintillations. However, this is not the case during 17 March 2013 wherein the TOI is seen to be continuous and could be the reason for lower scintillation activity during the late main phase of the storm on this day.

Although the surges in the TEC at Bharati and Davis appeared at similar time intervals suggesting that the ionospheric plasma density behaves in a similar manner for equivalent geophysical conditions, the magnitude of enhancements in the TEC on both the days is different. Interestingly, the magnitude of the increase in the TEC correlates with the intensity of the geomagnetic storm. While the minima of Sym-H on 17 March 2013 was approximately -135 nT and the increase in the midnight TEC was about 10 TECu, the minima in Sym-H on 17 March 2015 were approximately -230 nT, and the corresponding increase in the TEC during midnight was about $\sim$20 TECu. In order to understand the reasons for the presence of enhanced plasma content in the TOI during the storm of 17 March 2015 as compared to 17 March 2013 and the possible correlation with the intensity of the geomagnetic storm, we examine (1) the possible mechanisms that led to the formation of the TOI in the southern polar ionosphere and (2) the role of external driving mechanisms in modulating the IT response during both these events.

5.1. Mechanisms for the Formation of TOI/SED

The SEDs are longitudinally narrow regions of high TEC formed by a combination of mechanisms primarily driven by the storm time electric fields (PPEF and SAPS) and neutral winds (Foster, 2008). The TOI is known to form as a result of the antisunward convection of plasma from the region of SEDs across the polar cap and into the midnight auroral zone (Foster et al., 2005). The electric fields generated through the solar wind-magnetosphere coupling and mapped into the high-latitude regions along the magnetic field lines cause the expansion of the high-latitude convection cell to lower latitudes farther beyond the composition disturbance zone (Cowley, 2000; Foster, 2008). Studies have shown that the continuous expansion of the high-latitude convection cell to lower latitudes in response to the PPEF leads to the buildup of high-density solar photo-ionized plasma along the equatorward edge of the convection cell resulting in the formation of SEDs (Foster, 2008). DMSP observations (see Figures 5 and 6) of the auroral ionosphere show the large expansion of the auroral oval to lower latitudes in response to the southward turning of IMF on both 17 March 2013 and 17 March 2015. On 17 March 2013, the most extended aurora had its equatorward boundary at 56°S MLAT. The 17 March 2015 storm event had more dramatic ionospheric effects with the appearance of the most extended aurora with its equatorward boundary at latitudes $\sim$5° lower than that observed on 17 March 2013. Using DMSP observations, Hairston et al. (2016) showed that the convection pattern reached as low as 30°S MLAT on the duskside and 40°S MLAT on the dawnside during the main phase of the storm on 17 March 2015. These observations clearly suggest that the regions of SED formation on 17 March 2015 are located at lower latitudes, that is, at regions of higher solar photo-ionized plasma density.

The TEC in the midlatitude regions may also enhance under the action of PPEF. Since the high-latitude electric fields penetrate almost simultaneously to the middle, low, and equatorial latitudes, the signature of the PPEF can be inferred from ground magnetic field variations at low latitudes (Anderson et al., 2002). Here, we examine the nature of low-latitude electric fields on 17 March 2013 and 17 March 2015 as a signature of the PPEF and discuss its possible contribution to the formation of SEDs on these two days. Figures 10a and 10b show the EEJ strength (black line) during 17 March 2013 and 17 March 2015 respectively along with the variation of EEJ on a quiet day (brown line) in March in the respective years. The EEJ measurements shown here are obtained from the Indian sector which lies in the similar longitude sector as the Antarctic stations, Bharati and Davis. Sudden enhancements in the EEJ strength are observed starting at about $\sim$0600 UT and in the early main phase of the storms on 17 March 2013 as well as 17 March 2015. This indicates the presence of strong eastward electric field in the equatorial ionosphere on these days. The EEJ strength on 17
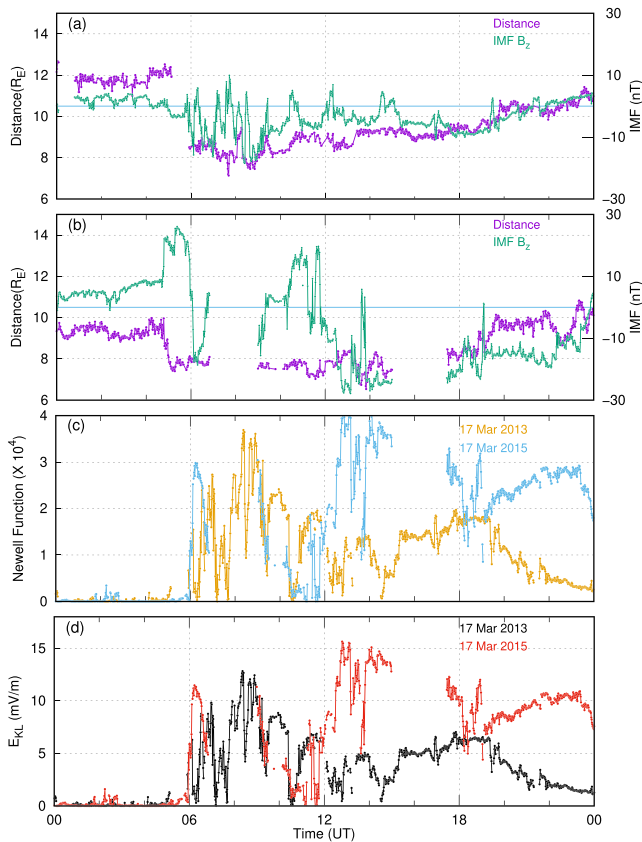
Figure 11. Panels (a) and (b) represent the temporal variation of the magnetopause and the IMF B_z on 17 March 2013 and 17 March 2015, respectively. Panel (c) represents the variation of the Newell function on 17 March 2013 (shown in brown) and 17 March 2015 (shown in blue), respectively. Panel (d) represents the variation of the reconnection electric field on 17 March 2013 (shown in black) and 17 March 2015 (shown in red), respectively.

March 2015 started to increase at ~0545 UT and reached the magnitude of ~120 nT to decrease in about 45 min. There are other enhancements in the EEJ strength during 0630–0830 UT on this day but of lower magnitude. The presence of enhanced dayside upward flows in the equatorial ionosphere on 17 March 2015 has been reported by Hairston et al. (2016) consistent with the EEJ variations. The EEJ strength on 17 March 2013, on the other hand, is of lower magnitude (<100 nT) as compared to that on 17 March 2015 and is mostly fluctuating probably in response to the fluctuating IMF B_z. These evidences show the prevalence of stronger PPEF on 17 March 2015 as compared to that on 17 March 2013. The stronger PPEF on 17 March 2015, which is eastward in direction during daytime when combined with the daytime midlatitude ionospheric electric fields, produces larger upward and poleward ExB plasma drifts thereby leading to an increase in the midlatitude electron density.

The midlatitude ionospheric densities are also known to be enhanced by the action of the neutral winds during disturbed times (Balan et al., 2010). GUVI observations (shown in Figure 7) show that the decrease of O/N_2 ratio over the high latitudes on 17 March 2015 is also accompanied by a huge visible increase in the O/N_2 ratio over the southern midlatitude regions. This feature is present on 17 March 2013 also but of lower magnitude. Such large changes in the O/N_2 ratio are known to take place as (1) the strong joule heating at high latitudes induces the upwelling of air rich in molecular species to higher altitudes thereby reducing the O/N_2 ratio, (2) the downwelling air at low-midlatitudes brings atomic constituents to low altitudes thereby increasing the O/N_2 ratio. Hence, from a comparison of the O/N_2 observations on both storm days, it can be inferred that on 17 March 2015, stronger equatorward neutral winds were prevalent in the southern high-midlatitude regions and led to larger enhancements in the O/N_2 ratio over the southern midlatitude regions. Consequently, one can expect the presence of high TEC in the southern midlatitude regions during the storm event of 17 March 2015 as compared to 17 March 2013. This is because the large increase in the O/N_2 ratio at midlatitude regions on 17 March 2015 could lead to lower recombination rates

in the F region altitudes of the ionosphere and therefore cause a subsequent increase in the TEC. The storm-induced neutral winds that are equatorward in direction also act to push the ionosphere to higher altitudes along the inclined magnetic field lines in the midlatitude regions (Balan et al., 2010). This further leads to lower recombination rates in the F region altitudes of the ionosphere and leads to an increase in the plasma density in the midlatitude regions.

From the above discussions, it is clear that the presence of stronger PPEF during the early main phase of the storm on 17 March 2015 (1) led to the larger expansion of the high-latitude convection cell to regions of high-density solar photo-ionized plasma and (2) led to the enhanced upward and poleward ExB drifts in the midlatitude ionosphere. These processes led to the presence of higher plasma content in the regions of SED formation on 17 March 2015 as compared to those on 17 March 2013. Further, the presence of stronger storm-induced equatorward neutral winds on 17 March 2015 aided the enhancement of midlatitude ionospheric densities thereby contributing to the enhancement of plasma content in the SEDs. The strong SAPS electric field acting over the subauroral latitudes in combination with strong antisunward convection across the polar cap led to the formation of the high-density TOI on 17 March 2015. As described earlier, these phenomena were weaker during the storm of 17 March 2013 as compared to that on 17 March 2015 thereby resulting in the formation of a comparatively low-density polar TOI.

5.2. Role of External Driving Mechanisms

It is well known that the intensity of a geomagnetic storm is a function of the solar wind driving conditions and the orientation of the IMF (Gonzalez et al., 1994). In order to put our observations into perspective and

understand how the differences in the degree of external forcing during the St. Patrick's Day storms of 2013 and 2015 led to the observed IT response on the respective storm days, we make use of the different formulations that describe interaction of the solar wind with the magnetosphere-ionosphere system. For this purpose, we examined the variation of magnetopause distance, Kan-Lee reconnection electric field E_{KL} (Kan & Lee, 1979) and Newell function (Newell et al., 2007) on these two days. The magnetopause standoff distance during 17 March 2013 and 17 March 2015 calculated to the first order by using the pressure balance equation described by Roelof and Sibeck (1993) is shown in Figures 11a and 11b along with the IMF B_z. The rate of magnetic flux opened at the dayside magnetopause represented by the Newell function is shown in Figure 11c. It is calculated as

$$\frac{d\phi}{dt} = v^{4/3} B_{T}^{2/3} sin^{8/3}(\theta_c/2) \tag{1}$$

where v is the solar wind speed, B_T is the magnitude of transverse IMF, and θ_c is the IMF clock angle.

The Kan-Lee electric field E_{KL} that quantifies the reconnection of the IMF at high latitudes is shown in Figure 11d. The Kan-Lee electric field reconnection electric field E_{KL} is calculated as

$$E_{KL} = v B_T sin^2(\theta_c/2) \tag{2}$$

where v is the solar wind speed, B_T is the magnitude of transverse IMF, and θ_c is the IMF clock angle.

It is seen from Figures 11a and 11b that the magnetopause standoff distance has moved to regions closer to the Earth ($\sim 8\ R_E$) immediately after the SSC on both 17 March 2013 and 17 March 2015. This can be attributed to the sudden enhancement in the solar wind velocities (700 and 500 km/s) and pressure (20 and 10 nPa) at $\sim$0600 UT on 17 March 2013 and $\sim$0545 UT 17 March 2015, respectively (see Figure 1). It is known that the magnetopause moves earthward in order to maintain the balance between the solar wind dynamic pressure and the magnetospheric pressure. Under these conditions, if the IMF is southward in direction, then the dayside magnetic reconnection drives the erosion of magnetic flux (Aubry et al., 1970). A comparison of the magnetopause standoff distances in Figures 11a and 11b shows that during the St. Patrick's Day storm of 2015, the magnetopause erosion sustained for a longer time (13 hr) as compared to that on 17 March 2013. Further, the rate of magnetic flux opened at the dayside magnetopause (Figure 11c) and the reconnection electric field (E_{KL}) (Figure 11d) exhibit large enhancements simultaneous to the southward turning of IMF during 0600 UT on 17 March 2015. Although of lesser magnitude and fluctuating in nature, the coupling function and the reconnection electric field are seen to increase during the period 0600–0700 UT on 17 March 2013. The low-latitude PPEF also exhibits similar trends as the reconnection electric field E_{KL} during the period 0600–0700 UT on both 17 March 2013 and 17 March 2015 (see Figure 10). Studies have shown that the reconnection electric field E_{KL} at the magnetopause is connected to the PPEF via the region 1 currents (Nopper Jr. & Carovillano, 1978). Our observations further confirms that the stronger PPEF on 17 March 2015 is connected to the presence of stronger reconnection electric field and emphasizes the direct control of the solar wind on the ionospheric system through storm time electric fields during the initial phases of the storm.

On both the storm days, the coupling is seen to reduce after 1000 UT owing to the northward turning of IMF B_z (see Figure 1) simultaneous to which the Sym-H index is also seen to recover from the point of first minima. However, at $\sim$1200 UT on 17 March 2015, in response to the southward turning of IMF B_z also accompanied by a second increase in the solar wind velocity, density, and pressure, there are large enhancements in the coupling and the reconnection electric field as obvious from Figure 11. The magnitude of reconnection electric field is seen to be greater than 10 mV/m during this period where the Sym-H drops further to its second minima of -223 nT. Previous studies have shown that periods with the magnitude of E_{KL} exceeding 10 mV/m for a duration of at least 10 min are to be highly disturbed (Mannucci et al., 2014). Hence, it is clear that the St. Patrick's storm of 2015 was a highly disturbed period with stronger coupling of the solar wind-magnetosphere-ionosphere system especially during the late main phase of the storm. Our observations showed complex flows in the polar cap, large equatorward expansion of the auroral oval, enhanced particle precipitation, strong SAPS electric fields, strong storm-induced equatorward neutral winds, and related ionospheric phenomena during the late main phase of the storm on 17 March 2015. This is unlike the case on 17 March 2013 where the magnitude of E_{KL} goes beyond 10 mV/m only for a short period ($\sim$1 hr) during

0800–0900 UT making it a geomagnetic storm period of lesser intensity. Further, on 17 March 2013, only smaller enhancements in the coupling and the E_{KL} in correspondence with periods of southward fluctuations in IMF are observed after 1200 UT, that is, in the late main phase of the storm.

We conclude that the differences in the duration and extent of magnetopause erosion caused the stronger response of the high-latitude ionosphere during the St. Patrick's Day of 2015. In this context, the large enhancement in the polar cap TEC at Bharati and Davis during the St. Patrick's Day storm of 2015 is proposed to be a result of the continuous enhancement of the polar TOI due to the prevalence of storm time electric fields and particle precipitation led by strong and long-lived magnetopause erosion. The same for the St. Patrick's Day storm of 2013 was weak and short-lived due to the fast fluctuating nature of the IMF B_z. In other words, as the IMF kept on changing its polarity (of Figure 1a) on 17 March 2013, the dayside reconnection weakened followed by slow reverting of the magnetopause standoff distance. The storm-induced electric fields, particle precipitation, and related phenomena weaken under these conditions. These results further confirm the fact that the external driving mechanisms play a very important role in modulating the storm time response of the high-midlatitude ionosphere.

6. Summary and Conclusions

Understanding the response of the terrestrial ionosphere to space weather events is important due to its effects on the performance of ground based and space based technology. The St. Patrick's Day storms of 2013 and 2015 provided an unique opportunity to gain insight into the causative connection between the external driving forces and the ionospheric phenomena that lead to the plasma density variations/irregularities in the polar ionosphere. The response of the southern polar ionosphere to these storms has been studied in this paper using ground-based GPS TEC and DMSP satellite measurements. During the main phase of the storms of 17 March 2013 and 17 March 2015, the TEC at the Antarctic stations, Bharati and Davis, evolved in a similar manner with enhancements in the TEC (positive ionospheric storms) at two distinct time zones, that is, in the local magnetic noon and midnight sectors. The positive ionospheric storms at Bharati and Davis that appear during the magnetic noon/midnight periods are topside TEC enhancements associated with the formation of SEDs/TOI. The daytime positive ionospheric storm at Bharati and Davis (while they are located in the cusp region) occurs as the SED plumes generated at the southern midlatitude region enter the cusp region, while the positive ionospheric storms observed during nighttime (while the stations are located in the polar cap) are a result of the formation of the TOI as the SED plumes extend into the polar cap through the polar cusp. Since the storm-induced neutral winds act to reduce the bottomside ionospheric densities at the southern polar regions, the contributions to the TEC enhancements at Bharati and Davis mainly come from the topside ionosphere. Hence, the storm time electric fields played an important role in generating the positive ionospheric storms at the polar cap regions during the St. Patrick's Day storms of 2013 and 2015. At Bharati, the periods of enhanced TEC were also colocated with periods of enhanced phase scintillation. The phase scintillations observed in the magnetic noon/midnight sector appeared due to the ionospheric irregularities generated by the enhanced particle precipitation and ionospheric convection on both the days.

The midnight enhancement in the TEC on 17 March 2015 was substantially larger in magnitude as compared to that observed on 17 March 2013 and varied in line with the intensity of the geomagnetic storm. The St. Patrick's Day storm of 2015 was a highly disturbed period with strong coupling of the SWMI system during the entire main phase of the storm. The presence of enhanced plasma density in the TOI formed in the southern polar cap on 17 March 2015 is a result of the complex coupling of the solar wind-magnetosphere-ionosphere system through electric fields and neutral winds for long durations. The strong and sustained magnetopause erosion on 17 March 2015 led to the prevalence of stronger storm time electric fields starting from the early main phase of the storm. The action of storm-induced neutral winds at the midlatitudes also favored the formation of higher plasma densities in the regions of SED formation during the main phase of the 17 March 2015 storm. This was not the case during the St. Patrick's Day storm of 2013 because magnetopause erosion is sustained for a much shorter period mainly due to fluctuating nature of IMF B_z with only small enhancements in the coupling function during the late main phase of the storm on 17 March 2013. Hence, the TEC enhancements observed in the polar cap ionosphere during the magnetic midnight period on 17 March 2013 are of lower magnitude. This study shows that the duration and extent of magnetopause

erosion play an important role in the spatiotemporal evolution of the plasma density distribution in the high-midlatitude ionosphere. This study highlights the fact that the behavior of the polar ionosphere is strongly influenced by the external drivers of geomagnetic storms and provides insight into the nature of interaction of the solar wind with the terrestrial IT system during the St. Patrick's Day of 2013 and 2015.

Data Availability Statement

These data sets are available at http://cdaweb.gsfc.nasa.gov, and http://wdc.kugi.kyoto-u.ac.jp, http://guvi-timed.jhuapl.edu. The DMSP particle fluxes and IDM data were obtained from the NOAA data center (http://www.ngdc.noaa.gov/stp/satellite/dmsp/). The GPS data from Bharati used in the paper are available online at spl.gov.in/SPL/INSWIM. The GPS data corresponding to Davis station are obtained from the IGS website (ftp://cddis.gsfc.nasa.gov; http://ftp.aiub.unibe.ch/CODE/). Data for TEC processing are provided from the following organizations: UNAVCO, Scripps Orbit and Permanent Array Center, Institut Geographique National, France, International GNSS Service, The Crustal Dynamics Data Information System (CDDIS), National Geodetic Survey, Instituto Brasileiro de Geografia e Estatstica, RAMSAC CORS of Instituto Geográfico Nacional de la República Argentina, Arecibo Observatory, Low-Latitude Ionospheric Sensor Network (LISN), Topcon Positioning Systems, Inc., Canadian High Arctic Ionospheric Network, Centro di Ricerche Sismologiche, Système d'Observation du Niveau des Eaux Littorales (SONEL), RENAG: REseau NAtional GPS permanent, GeoNet - the official source of geological hazard information for New Zealand, GNSS Reference Networks, Finnish Meteorological Institute, and SWEPOS - Sweden. Access to these data is provided by Madrigal network via http://cedar.openmadrigal.org/. The DMSP SSUSI data are available at https://ssusi.jhuapl.edu/.

References

Aarons, J. (1997). Global positioning system phase fluctuations at auroral latitudes. *Journal of Geophysical Research*, *102*, 17,219–17,231.

Anderson, D., Anghel, A., Yumoto, K., Ishitsuka, M., & Kudeki, E. (2002). Estimating daytime vertical ExB drift velocities in the equatorial F-region using ground-based magnetometer observations. *Geophysical Research Letters*, *29*(12), 1596. https://doi.org/10.1029/2001GL014562

Astafyeva, E., Zakharenkova, I., & Forster, M. (2015). Ionospheric response to the 2015 St. Patrick's Day storm: A global multi-instrument overview. *Journal of Geophysical Research: Space Physics*, *120*, 9023–9037. https://doi.org/10.1002/2015JA021629

Aubry, M. P., Russel, C. T., & Kivelson, M. G. (1970). Inward motion of the magnetopause before a substorm. *Journal of Geophysical Research*, *75*, 7018–7031. https://doi.org/10.1029/JA075i034p07018

Balan, N., Shiokawa, K., Otsuka, Y., Kikuchi, T., Lekshmi, D. V., Kawamura, S., et al. (2010). A physical mechanism of positive ionospheric storms at low and midlatitudes. *Journal of Geophysical Research*, *115*, A02304. https://doi.org/10.1029/2009JA014515

Buonsanto, M. J. (1999). Ionospheric storms-Review. *Space Science Reviews*, *88*, 563–601.

Cherniak, I., & Zakharenkova, I. (2016). High-latitude ionospheric irregularities: Differences between ground- and space-based GPS measurements during the 2015 St. Patrick's Day storm. *Earth, Planets and Space*, *68*(1), 136. https://doi.org/10.1186/s40623-016-0506-1

Chisham, G., Lester, M., Milan, S. E., Freeman, M. P., Bristow, W. A., Grocott, A., et al. (2007). A decade of the Super Dual Auroral Radar Network (SuperDARN): scientific achievements, new techniques and future directions. *Surveys in Geophysics*, *28*(1), 33–109. https://doi.org/10.1007/s10712-007-9017-8

Christensen, A. B. (2003). Initial observations with the Global Ultraviolet Imager (GUVI) in the NASA TIMED satellite mission. *Journal of Geophysical Research*, *108*(A12), 1451. https://doi.org/10.1029/2003JA009918

Clausen, L. B. N., Baker, J. B. H., Ruohoniemi, J. M., Milan, S. E., Coxon, J. C., Wing, S., et al. (2013). Temporal and spatial dynamics of the regions 1 and 2 Birkeland currents during substorms. *Journal of Geophysical Research: Space Physics*, *118*, 3007–3016. https://doi.org/10.1002/jgra.50288

Correia, E., Spogli, L., Alfonsi, L., Cesaroni, C., Gulisano, A. M., Thomas, E. G., et al. (2017). Ionospheric F-region response to the 26 September 2011 geomagnetic storm in the Antarctica American and Australian sectors. *Annales Geophysicae*, *35*, 1113–1129. https://doi.org/10.5194/angeo-35-1113-2017

Cowley, S. W. H. (2000). Magnetosphere-ionosphere interactions: A tutorial review. In S.-I. Ohtani, R. Fujii, M. Hesse, & R. L. Lysak (Eds.), *Magnetospheric current systems*. https://doi.org/10.1029/GM118p0091

Cowley, S. W. H., & Lockwood, M. (1992). Excitation and decay of solar wind-driven flows in the magnetosphere-ionosphere system. *Annales de Geophysique*, *10*, 103–115.

Dang, T., Lei, J., Wang, W., Wang, B., Zhang, B., Liu, J., et al. (2019). Formation of double tongues of ionization during the 17 March 2013 geomagnetic storm. *Journal of Geophysical Research: Space Physics*, *124*, 10,619–10,630. https://doi.org/10.1029/2019JA027268

Dmitriev, A. V., Suvorova, A. V., Klimenko, M. V., Klimenko, V. V., Ratovsky, K. G., Rakhmatulin, R. A., & Parkhomov, V. A. (2017). Predictable and unpredictable ionospheric disturbances during St. Patrick's Day magnetic storms of 2013 and 2015 and on 8-9 March 2008. *Journal of Geophysical Research: Space Physics*, *122*, 2398–2423. https://doi.org/10.1002/2016JA023260

Elphinstone, R. D., Murphree, J. S., & Cogger, L. L. (1996). What is a global auroral substorm? *Reviews of Geophysics*, *34*, 169–232.

Foster, J. C. (2008). Ionospheric-magnetospheric-heliospheric coupling: Storm-time thermal plasma redistribution. *Geophysical Monograph Series*, *181*, 121–134. https://doi.org/10.1029/181GM12

Foster, J. C., & Burch, W. J. (2002). SAPS: A new categorization for sub-auroral electric fields. *EOS*, *83*(36), 393–394.

Foster, J. C., Coster, A. J., Erickson, P. J., Holt, J. M., Lind, F. D., Rideout, W., et al. (2005). Multiradar observations of the polar tongue of ionization. *Journal of Geophysical Research*, *110*, A09S31. https://doi.org/10.1029/2004JA010928

Foster, J. C., Coster, A. J., Erickson, P. J., Rich, F. J., & Sandel, B. R. (2014). Stormtime observations of the flux of plasmaspheric ions to the dayside cusp/magnetopause. *Geophysical Research Letters*, *31*, L08809. https://doi.org/10.1029/2004GL020082

Foster, J. C., Erickson, P. J., Baker, D. N., Claudepierre, S. G., Kletzing, C. A., Kurth, W., et al. (2013). Prompt energisation of relativistic and highly relativistic electrons during a substorm interval: Van Allen Probes Observations. *Geophysical Research Letters*, *41*, 20–25. https://doi.org/10.1002/2013GL058438

Gonzalez, W. D., Joselyn, J. A., Kamide, Y., Kroehl, H. W., Rostoker, G., Tsurutani, B. T., & Vasyliunas, V. M. (1994). What is a geomagnetic storm. *Journal of Geophysical Research*, *99*(A4), 5771–5792.

Hairston, M., Coley, W. R., & Stoneback, R. (2016). Responses in the polar and equatorial ionosphere to the March 2015 St. Patrick Day storm. *Journal of Geophysical Research: Space Physics*, *121*, 11,213–11,234. https://doi.org/10.1002/2016JA023165

Joshi, L. M., Sripathi, S., & Singh, R. (2016). Simulation of low-latitude ionospheric response to 2015 St. Patrick's Day super geomagnetic storm using ionosonde-derived PRE vertical drifts over Indian region. *Journal of Geophysical Research*, *121*, 2489–2502. https://doi.org/10.1002/2015JA021512

Kan, J. R., & Lee, L. C. (1979). Energy coupling function and solar wind-magnetosphere dynamo. *Geophysical Research Letters*, *6*(7), 577–580. https://doi.org/10.1029/GL006i007p00577

Klimenko, M. V., Zakharenkova, I. E., Klimenko, V. V., Lukianova, R. Y., & Cherniak, I. V. (2019). Simulation and observations of the polar tongue of ionization at different heights during the 2015 St. Patrick's Day storms. *Space Weather*, *17*, 1073–1089. https://doi.org/10.1029/2018SW002143

Knudsen, W. C. (1974). Magnetospheric convection and the high-latitude F_2 ionosphere. *Journal of Geophysical Research*, *79*, 1046–1055.

Le, G., Luhr, H., Anderson, B. J., Strangeway, R. J., Russell, C. T., Singer, H., et al. (2016). Magnetopause erosion during the 17 March 2015 magnetic storm: Combined field-aligned currents, auroral oval, and magnetopause observations. *Geophysical Research Letters*, *43*, 2396–2404. https://doi.org/10.1002/2016GL068257

Liu, J., Wang, W., Burns, A., Solomon, S. C., Zhang, S., Zhang, Y., & Huang, C. (2016). Relative importance of horizontal and vertical transports to the formation of ionospheric storm-enhanced density and polar tongue of ionization. *Journal of Geophysical Research: Space Physics*, *121*, 8121–8133. https://doi.org/10.1002/2016JA022882

Liu, J., Wang, W., Burns, A., Yue, X., Zhang, S., Zhang, Y., & Huang, C. (2016). Profiles of ionospheric storm-enhanced density during the 17 March 2015 great storm. *Journal of Geophysical Research: Space Physics*, *121*, 727–744. https://doi.org/10.1002/2015JA021832

Lockwood, M., & Cowley, S. W. H. (1992). Ionospheric convection and the substorm cycle. In C. Mattock (Ed.), *Substorms 1, Proceedings of the First International Conference on Substorms, ICS-1, Kiruna, Sweden* (pp. 99–109). ESA-SP-335, ESA Special Publication SP 335 European Space Agency Publications, Nordvijk, The Netherlands ISBN 929092182X, 9789290921820.

Mannucci, A., Crowley, G., Tsurutani, B., Verkhoglyadova, O., Komjathy, A., & Stephens, P. (2014). Interplanetary magnetic field B_y control of prompt total electron content increases during superstorms. *Journal of Atmospheric and Solar-Terrestrial Physics*, *115-116*, 7–16. https://doi.org/10.1016/j.jastp.2014.01.001

Meng, C. I. (1970). Variation of the magnetopause position with substorm activity. *Journal of Geophysical Research*, *75*, 3252.

Mitchell, C. N., Alfonsi, L., DeFranceschi, G., Lester, M., Romano, V., & Wernik, A. W. (2005). GPS TEC scintillation measurements from the polar ionosphere during the October 2003 storm. *Journal of Geophysical Research*, *32*, L12S03. https://doi.org/10.1029/2004GL021644

Moen, J., Oksavik, K., Alfonsi, L., Daabakk, Y., Romano, V., & Spogli, L. (2013). Space weather challenges of the polar cap ionosphere. *Journal of Space Weather and Space Climate*, *3*, A02. https://doi.org/10.1051/swsc/2013025

Nava, B., Rodriguez-Zuluaga, J., Alazo-Cuartas, K., Kashcheyev, A., Migoya-Orue, Y., Radicella, S. M., et al. (2016). Middle- and low-latitude ionospheric response to 2015 St. Patrick's Day geomagnetic storm. *Journal of Geophysical Research: Space Physics*, *121*, 3421–3438. https://doi.org/10.1002/2015JA022299

Newell, P. T., Sotirelis, T., Liou, K., Meng, C.-I., & Rich, F. J. (2007). A nearly universal solar wind-magnetosphere coupling function inferred from 10 magnetospheric state variables. *Journal of Geophysical Research*, *112*, A01206. https://doi.org/10.1029/2006JA012015

Nopper Jr., R. W., & Carovillano, R. L. (1978). Polar-equatorial coupling during magnetically active periods. *Geophysical Research Letters*, *5*(8), 699–702. https://doi.org/10.1029/GL005i008p00699

Paxton, L. J. (2005). Global Ultraviolet Imager (GUVI): Measuring composition and energy inputs for the NASA Thermosphere-Ionosphere-Mesosphere Energetics and Dynamics (TIMED) mission. *Proceedings of SPIE The International Society for Optical Engineering*, *3756*, 265–276.

Paxton, L. J., Meng, C. I., Fountain, G. H., Ogorzalek, B. S., Darlington, E. H., Goldstein, J., & Peacock, K. (1992a). SSUSI: Horizon-to-horizon and limb viewing spectrographic imager for remote sensing of environmental parameters. *Proceedings SPIE*, *1764*, 161. https://doi.org/10.1117/12.140846

Paxton, L. J., Meng, C. I., Fountain, G. H., Ogorzalek, B. S., Darlington, E. H., Goldstein, J., et al. (1992b). Special sensor UV spectrographic imager (SSUSI): An instrument description. *Instrument Planetary Terrestrial, Atmospheric Remote Sensing*, *1745*, 2.

Prölss, G. W. (1995). Ionospheric F-region storms. In H. Volland (Ed.), *Handbook of atmospheric electrodynamics* (Vol. 2, pp. 195–248).

Ramsingh, S., Sreekumar, S., Banola, S., Emperumal, K., Tiwari, P., & Kumar, B. S. (2015). Sripathi low-latitude ionospheric response to super geomagnetic storm of 17/18 March 2015: Results from a chain of ground-based observations over Indian sector. *Journal of Geophysical Research: Space Physics*, *120*, 10,864–10,882. https://doi.org/10.1002/2015JA021509

Rastogi, R. G., & Klobuchar, J. A. (1990). Ionospheric electron content within the equatorial F2 layer anomaly belt. *Journal of Geophysical Research*, *95*(19), 045.

Rideout, W., & Coster, A. (2006). Automated GPS processing for global total electron content data. *GPS Solutions*, *10*(3), 219–228. https://doi.org/10.1007/s10291-006-0029-5

Rodger, C. D., Taylor, F. W., Muggeridge, A. H., Lopez-Puertas, M., & Lpoez-Valverde, M. A. (1992). Local thermodynamic equilibrium of carbon dioxide in the upper atmosphere. *Geophysical Research Letters*, *19*, 589–592.

Roelof, E. C., & Sibeck, D. G. (1993). Magnetopause shape as a bivariate function of interplanetary magnetic field B_z and solar wind dynamic pressure. *Journal of Geophysical Research*, *98*, 421–450.

Schunk, R. W., & Nagy, A. F. (2000). *Cambridge Atmospheric and Space Science Series* (Vol. 59). Cambridge: Cambridge University Press. https://doi.org/10.1017/CBO9780511551772

Shreedevi, P. R., & Choudhary, R. K. (2017). Impact of oscillating IMF B_z during 17 March 2013 storm on the distribution of plasma over Indian low-latitude and mid-latitude ionospheric regions. *Journal of Geophysical Research: Space Physics*, *122*, 607–623. https://doi.org/10.1002/2017JA023980

Shreedevi, P. R., Choudhary, R. K., Yiqun, Y., & Thomas, E. G. (2019). Morphological study on the ionospheric variability at Bharati: A polar cusp station in the Southern Hemisphere. *Journal of Atmospheric and Solar-Terrestrial Physics*, *193*, 105,058. https://doi.org/10.1016/j.jastp.2019.105058

Shreedevi, P. R., Thampi, S. V., Chakrabarty, D., Choudhary, R. K., Pant, T. K., Bhardwaj, A., & Mukherjee, S. (2016). On the latitudinal changes in ionospheric electrodynamics and composition based on observations over the 76-77°E meridian from both hemispheres during a geomagnetic storm. *Journal of Geophysical Research: Space Physics*, *121*, 1557–1568. https://doi.org/10.1002/2015JA021841

Smith, D. A., Araujo-Pradere, E. A., Minter, C., & Fuller-Rowell, T. (2008). A comprehensive evaluation of the errors inherent in the use of a two-dimensional shell for modeling the ionosphere. *Radio Science*, *43*, RS6008. https://doi.org/10.1029/2007RS003769

Sojka, J. J., Bowline, M. D., Schunk, R. W., Decker, D. T., Valladares, C. E., Sheehan, R., et al. (1993). Modeling polar cap F-region patches using time varying convection. *Geophysical Research Letters*, *20*, 1783.

Spogli, L., Alfonsi, L., Franceschi, G. D., Romano, V., Aquino, M. H. O., & Dodson, A. (2009). Climatological of GPS scintillations over high and mid-latitude European regions. *Annales de Geophysique*, *27*, 3429–3437.

St-Maurice, J. P., & Torr, D. G. (1978). Nonthermal rate coefficients in the ionosphere: The reactions of O^+ with N2, O2, and NO. *Journal of Geophysical Research*, *83*, 969–977.

Thomas, E. G., Baker, J. B. H., Ruohoniemi, J. M., Clausen, L. B. N., Coster, A. J., Foster, J. C., & Erickson, P. J. (2013). Direct observations of the role of convection electric field in the formation of a polar tongue of ionization from storm enhanced density. *Journal of Geophysical Research: Space Physics*, *118*, 1180–1189. https://doi.org/10.1002/jgra.50116

Tulasiram, S., Yokoyama, T., Otsuka, Y., Shiokawa, K., Sripathi, S., Veenadhari, B., et al. (2015). Duskside enhancement of equatorial zonal electric field response to convection electric fields during the St. Patrick's Day storm on 17 March 2015. *Journal of Geophysical Research: Space Physics*, *120*, 538–548. https://doi.org/10.1002/2015JA021932

Valladares, C. E., Carlson, H. C. J., & Fukui, K. (1994). Interplanetary magnetic field dependency of stable sun-aligned polar cap arcs. *Journal of Geophysical Research*, *99*(A4), 6247–6272.

Verkhoglyadova, O. P., Tsurutani, B. T., Mannucci, A. J., Mlynczak, M. G., Hunt, L. A., Paxton, L. J., & Komjathy, A. (2016). Solar wind driving of ionosphere-thermosphere responses in three storms near St.Patrick's Day in 2012, 2013, and 2015. *Journal of Geophysical Research: Space Physics*, *121*, 8900–8923. https://doi.org/10.1002/2016JA022883

Wei, D., Yu, Y., & He, F. (2019). The magnetospheric driving source of double-peak subauroral ion drifts: Double ring current pressure peaks. *Geophysical Research Letters*, *46*, 7079–7087. https://doi.org/10.1029/2019GL083186

Wei, D., Yu, Y., Ridley, A. J., Cao, J., & Dunlop, M. W. (2019). Multi-point observations and modeling of subauroral polarization streams (SAPS) and double-peak subauroral ion drifts (DSAIDs): A case study. *Advances in Space Research*, *63*(11), 3522–3535. https://doi.org/10.1016/j.asr.2019.02.004

Wernik, A. W., Alfonsi, L., & Materassi, M. (2007). Scintillation modeling using in situ data. *Radio Science*, *42*, RS1002. https://doi.org/10.1029/2006RS003512

Yadav, S., Sunda, S., & Sridharan, R. (2016). The impact of the 17 March 2015 St. Patrick's Day storm on the evolutionary pattern of equatorial ionization anomaly over the Indian longitudes using high-resolution spatio-temporal TEC maps: New insights. *Space Weather*, *14*, 786–801. https://doi.org/10.1002/2016SW001408

Yeh, H. C., Foster, J. C., Rich, F. J., & Swider, W. (1991). Storm-time electric field penetration observed at mid-latitude. *Journal of Geophysical Research*, *96*, 5707.

Yue, X., Wan, W., Liu, L., Liu, J., Zhang, S., Schreiner, W. S., et al. (2016). Mapping the conjugate and corotating storm-enhanced density during 17 March 2013 storm through data assimilation. *Journal of Geophysical Research: Space Physics*, *121*, 12,202–12,210. https://doi.org/10.1002/2016JA023038

Yue, X., Wang, W., Lei, J., Burns, A., Zhang, Y., Wan, W., et al. (2016). Long-lasting negative ionospheric storm effects in low and middle latitudes during the recovery phase of the 17 March 2013 geomagnetic storm. *Journal of Geophysical Research: Space Physics*, *121*, 9234–9249. https://doi.org/10.1002/2016JA022984

Zhang, S. R., Zhang, Y., Wang, W., & Verkhoglyadova, O. P. (2017). Geospace system responses to the St. Patrick's Day storms in 2013, and 2015. *Journal of Geophysical Research: Space Physics*, *122*, 6901–6906. https://doi.org/10.1002/2017JA024232